Federated Learning in Multi-RIS-Aided Systems

Wanli Ni, *Graduate Student Member, IEEE*, Yuanwei Liu, *Senior Member, IEEE*, Zhaohui Yang, *Member, IEEE*, Hui Tian, *Senior Member, IEEE*, and Xuemin Shen, *Fellow, IEEE*

***Abstract*—The fundamental communication paradigms in the next-generation mobile networks are shifting from connected things to connected intelligence. The potential result is that current communication-centric wireless systems are greatly stressed when supporting computation-centric intelligent services with distributed big data. This is one reason that makes federated learning come into being, it allows collaborative training over many edge devices while avoiding the transmission of raw data. To tackle the problem of model aggregation in federated learning systems, this article resorts to multiple reconfigurable intelligent surfaces (RISs) to achieve efficient and reliable learning-oriented wireless connectivity. The seamless integration of communication and computation is actualized by over-the-air computation (AirComp), which can be deemed as one of the uplink nonorthogonal multiple access (NOMA) techniques without individual information decoding. Since all local parameters are uploaded via noisy concurrent transmissions, the unfavorable propagation error inevitably deteriorates the accuracy of the aggregated global model. The goals of this work are to 1) alleviate the signal distortion of AirComp over shared wireless channels and 2) speed up the convergence rate of federated learning. More specifically, both the mean-square error (MSE) and the device set in the model uploading process are optimized by jointly designing transceivers, tuning reflection coefficients, and selecting clients. Compared to baselines, extensive simulation results show that 1) the proposed algorithms can aggregate model more accurately and accelerate convergence and 2) the training loss and inference accuracy of federated learning can be improved significantly with the aid of multiple RISs.**

***Index Terms*—Connected intelligence, nonorthogonal multiple access (NOMA), over-the-air federated learning (AirFL), reconfigurable intelligent surface (RIS), resource allocation.**

Manuscript received September 5, 2021; revised October 25, 2021; accepted November 19, 2021. Date of publication November 24, 2021; date of current version June 7, 2022. This work was supported in part by the National Key Research and Development Program of China under Grant 2018YFE0205502, and in part by the China Scholarship Council (CSC). This article was presented in part at the IEEE GLOBECOM Workshops, Taipei, Taiwan, December 2020. *(Corresponding author: Hui Tian.)*

Wanli Ni and Hui Tian are with the State Key Laboratory of Networking and Switching Technology, Beijing University of Posts and Telecommunications, Beijing 100876, China (e-mail: charleswall@bupt.edu.cn; tianhui@bupt.edu.cn).

Yuanwei Liu is with the School of Electronic Engineering and Computer Science, Queen Mary University of London, London E1 4NS, U.K. (e-mail: yuanwei.liu@qmul.ac.uk).

Zhaohui Yang is with the Department of Electronic and Electrical Engineering, University College London, London WC1E 6BT, U.K. (e-mail: zhaohui.yang@ucl.ac.uk).

Xuemin Shen is with the Department of Electrical and Computer Engineering, University of Waterloo, Waterloo, ON N2L 3G1, Canada (e-mail: sshen@uwaterloo.ca).

Digital Object Identifier 10.1109/JIOT.2021.3130444

I. Introduction

EMBRACING intelligence-based solutions is a pivotal step for the next-generation communication and networking systems to make the vision of a smarter world into reality [1], [2]. Usually, the traditional centralized learning methods are likely to bring a communication, computation, and storage burden at the base station (BS) [3], due to the massive connectivity of Internet of Things (IoT) devices in providing pervasive intelligent services [4]. To address this challenge, federated learning is emerged to achieve cost-efficient and learning-oriented networking in a distributive manner [5]. As one of the state-of-the-art candidates of distributed artificial intelligence, federated learning enables IoT-connected devices to build a global model collaboratively while keeping the privacy-sensitive personal data unmovable [6]–[8]. In this respect, federated learning features its unique strengths as compared to centralized machine learning paradigms [9], [10]. For example, first, federated learning allows data collected on different IoT devices to be used only locally, which effectively avoids the wireless transmission of raw data through a vulnerable air interface. This is greatly beneficial to preserve data security and user privacy in many information-critical applications [10]–[12].

In addition, only the up-to-date local model parameters need to be communicated with the BS [10], thus the communication overhead can be significantly reduced in federated learning. This also helps to alleviate the unbearable propagation delay caused by the potential traffic congestion and insufficient channel capacity [5]. Furthermore, harnessing the superposition property of wireless multiple-access channel (MAC), over-the-air computation (AirComp) can be adopted to complete the local parameter communication and global model computation processes in one concurrent transmission [13], [14]. Although AirComp and nonorthogonal multiple access (NOMA) have different objectives and performance metrics [15], both of them use the same time–frequency resources to serve multiple users from the perspective of the physical layer. Broadly speaking, AirComp without individual information decoding can be regarded as one of the uplink NOMA techniques [12], [16], and thus both the completion time and spectrum efficiency of the over-the-air federated learning (AirFL) system can be improved in comparison with the conventional orthogonal multiple access-based schemes [10], [17]. Finally, compared with the conventional cloud learning, federated learning is inherently conducive to offloading compute-intensive tasks from the central server to the edge devices [11], [18], which

can speed up the processing of real-time data by making full use of the dispersed computation resources at the network edge [3], [8]. However, because of the problems such as wireless signal distortion and global aggregation error brought by the resource-constrained IoT devices, it is very likely to worsen the training behavior of federated learning over the noisy fading channels. Therefore, it is important to design innovative, spectrum-efficient, and communication-efficient solutions for federated learning over IoT-connected intelligence networks.

By equipping a lot of low-cost passive reflecting elements on the digitally controllable metasurface, reconfigurable intelligent surfaces (RISs) make it possible to control the real-time waveform of the incident signal. Owing to the new dimensions introduced by RISs, this technological breakthrough has brought a revolutionary trend of thought to future network design. So far, RIS-aided communications have been recognized as one of the typical futuristic wireless technologies, due to the fact that programmable RISs are capable of flexibly reconfiguring the complicated wireless environment of radio signals in a broad range of frequency [19]. Not only can the propagation channels between the BS and users be proactively modified by tuning the reflection coefficient (including the amplitude and the phase shift) of each passive reflecting element but also no extra effort is needed to manage the sophisticated interference even though multiple RISs are considered [20]. Moreover, although traditional active relays that support multiple-input–multiple-output (MIMO) or millimeter-wave communication can achieve similar effects, RISs have better performance in terms of hardware cost and energy consumption [21]. Consequently, the software-controlled RISs are expected to provide a novel paradigm to create a smart and flexible wireless environment that can better satisfy the networking requirements of connected intelligence. Nevertheless, the ever-increasing complexity of wireless networks composed of a set of heterogeneous facilities makes effective modeling and networking difficult if not impossible. As a result, the efficient implementation of RIS-aided intelligent IoT networks also faces critical challenges from architecture design to system characterization and performance optimization [20]–[22].

Sparked by the aforementioned benefits and issues, it is imperative to merge AirFL with RIS for the reduced aggregation error and the faster convergence rate. The specific profits and reasons are given as follows.

1) First, the performance of AirFL can be improved by carefully designing the reflection coefficients at the RISs to make full use of the interference feature of MAC channels. Through aligning multiple signals via RISs, MAC channels can be deemed as a virtual computer capable of matching the desired aggregation function of AirFL. The efficient combination of communication and computation also helps to boost the spectrum utilization of resource-constrained IoT networks.
2) Then, the signal distortion of AirComp can be further reduced by deploying multiple RISs to merge reflected signals dexterously, so that the model parameters from local users can be aggregated more accurately. Another benefit of RISs is to provide available links for cell-edge users blocked by obstacles, thereby enhancing the coverage and connectivity of federated learning. After all, more learning participants with reliable channels can speed up the convergence rate of global aggregation.
3) Finally, compared to conventional active relays, RISs usually do not need dedicated battery supplies for operation. Therefore, RISs can be simply integrated into upcoming intelligence-connected networks without replacing any existing standard or hardware, so that the energy efficiency of learning-oriented IoT networks can be enhanced significantly without increasing huge extra operating expenses.

A. Challenges and Contributions

Since native intelligence is expected to play a defining role in the design of future networks, RIS-aided federated learning is an attractive candidate for actualizing the efficient integration of distributed learning and wireless communication. This caters to the fundamental needs of next-generation wireless networks supporting massive connectivities of edge intelligence. However, only a paucity of research attention has been given to the investigation of AirFL systems aided by intelligent surfaces, thereby motivating this work. So far, one challenge is that it is still intractable to minimize the mean-square error (MSE) of AirFL systems by jointly designing the transmit power, receive scalar, and reflection coefficients in a communication-efficient manner while guaranteeing the global aggregation error requirements within the available power budget. Moreover, another challenge is that the combinational optimization problem of device selection is usually nondeterministic polynomial-time (NP) hard.

In order to reduce the propagation error of wireless communication while speeding up the convergence rate of global aggregation, we investigate both the model synchronization and device selection problems in multi-RIS-aided AirFL systems. Notably, RISs play a significant role in turning the wireless channels into a functional computer to better match the desired weighted sum aggregation of federated learning. More precisely, multiple geodistributed RISs are deployed to enhance the parameter aggregation from IoT devices to the BS in an efficient manner. For the purpose of expanding our contributions, we consider both the single-antenna and multiantenna cases, in which the closed-form solutions and iterative algorithms are developed to obtain suboptimal solutions with a tradeoff between performance and complexity. To the best of our knowledge, RIS-aided AirFL is still at its nascent stage and many open issues remain to be addressed such as the joint design of transmit–reflect–receive in multi-RIS-aided IoT networks. The main contributions of this work are summarized as follows.

1) *Proposed Framework of Multi-RIS-Assisted AirFL:* We propose a framework of leveraging multiple RISs to reshape wireless channels into a virtual computer better matching the model aggregation function of AirFL. Accordingly, we formulate resource allocation and device selection problems for aggregation accuracy

enhancement and convergence rate improvement by jointly optimizing the transmit power, receive scalar, phase shifts, and learning participants, subject to power constraints at IoT devices and unit-modulus constraints at RISs, while satisfying the error tolerance of AirFL. The original problem is analyzed to be a mixed-integer nonlinear programming (MINLP) problem. Due to the NP-hard nature, a decomposition approach is adopted to solve the nonconvex problem in an iterative manner.

2) *Joint Optimization of Transceiver, Reflection, and Device Selection:* In order to tackle the MSE minimization subproblem with continuous variables, we first derive closed-form solutions for transceiver design in both single and multiantenna cases. Next, we use semidefinite relaxation (SDR) and successive convex approximation (SCA) to transform subproblems into convex ones and then solve them in polynomial time complexity. Afterward, we invoke difference-of-convex (DC) programming to handle the cardinality maximization subproblem with the combinatorial feature. Based on this, an alternating algorithm is developed to solve the MINLP problem.
3) *Experimental Validation and Discussion:* We conduct comprehensive simulations on the synthetic and real data sets to validate the effectiveness of the designed algorithms. Numerical results show that the proposed communication-efficient solutions for multi-RIS-assisted AirFL systems outperform benchmarks, such as single-RIS and random-phase schemes. Specifically, our algorithms can achieve a better convergence rate and lower learning error in the experiments of implementing AirFL for linear regression and image classification. Meanwhile, we verify that the deployment of RISs is beneficial to alleviate propagation error and reduce signal distortion of AirFL over shared wireless channels. Our schemes are also capable of reducing energy consumption and prolonging the overall lifetime of IoT networks.

B. Organization and Notations

The remainder of this article is organized as follows. First, the system model of multi-RIS-aided AirFL is given in Section III. Then, a bicriterion problem for learning behavior improvement is formulated in Section IV where the problem decomposition is conducted as well. Next, an alternating optimization algorithm for resource allocation and device selection is proposed in Section V. Finally, extensive numerical simulations are presented in Section VI, which is followed by the conclusion in Section VII.

The key notations of this article are summarized as follows. Scalars are denoted by italic letters, and vectors and matrices are denoted by boldface lowercase and uppercase letters, respectively. The space of $m \times n$ complex-valued matrices is denoted by $\mathbb{C}^{m\times n}$. The distribution of a complex Gaussian random vector with mean vector μ and covariance matrix σ^2 is denoted by $\mathcal{CN}(\mu, \sigma^2)$, and $\sim$ stands for "distributed as." For a complex number x, the amplitude is denoted by $|x|$. Meanwhile, $\mathrm{Re}(x)$ and $\mathrm{Im}(x)$ denote the real and imaginary parts of x, respectively. For a complex vector $\boldsymbol{x}$, $\mathrm{diag}(\boldsymbol{x})$ denotes a diagonal matrix with each diagonal element being the corresponding element in $\boldsymbol{x}$.

II. Related Works

Presently, with the development of wireless communication along with machine learning technologies, both federated learning and RISs are getting remarkable attention from academia and industry [2], [9]. Whereas, the majority of previous works only considered the separate implementation in simplex application scenarios where RIS-aided communication [21] and machine learning [10] were two decoupled areas. Due to the decentralized feature of the data samples and computation resources in mobile networks, a lot of prior literature, such as [20] and [23]–[29], aimed at investigating wireless communications for distributed intelligence from the perspectives of theoretical analysis and resource allocation. For instance, in an effort to strike a tradeoff between energy consumption and completion time at the network edge, Yang *et al.* [20] studied an energy-efficient resource allocation problem for frequency-domain multiple access-based federated learning systems. In order to shorten the communication latency, Zhu *et al.* [16] proposed a broadband transmission scheme for analog federated learning, which outperformed the conventional orthogonal access. Through implementing distributed stochastic gradient descent (SGD) for parameter updating, Amiri and Gündüz [25] proposed digital and analog communication schemes for federated learning over a shared bandwidth-limited noisy MAC. Furthermore, combating with the nonstationary gradient updates in different training rounds, Guo *et al.* [14] redesigned the AirFL transceiver and SGD learning rate over the time-varying fading channels. Similarly, an importance and channel-aware scheduling scheme was proposed in [30] to take advantage of the diversities brought by multiuser wireless communication and personalized local learning.

As for the wireless data aggregation techniques, a major design goal is to minimize the global MSE value under power constraints at edge devices, which is also applicable to the model aggregation in AirFL scenarios [14], [29]. Specifically, taking both the intranode interference and the nonuniform fading into account, Chen *et al.* [27] analyzed the aggregation performance of AirComp and derived the closed-form expression of the MSE outage, then receive antenna selection was adopted to avoid massive channel state information (CSI) gathering in the MIMO networks. Then, exploiting the functional decomposition, Liu *et al.* [28] focused on the MSE minimization problem of AirComp by designing the transceiver policy under the power constraint, where the closed-form expressions for computation-optimal strategy were derived. Moreover, by integrating the wireless-powered transfer and AirComp techniques, Li *et al.* [31] jointly optimized downlink energy transfer, uplink power control, and receiver beamforming to minimize the aggregation error of distributed sensing data.

Additionally, a large number of previous studies have focused on the basic challenging problems in RIS-aided

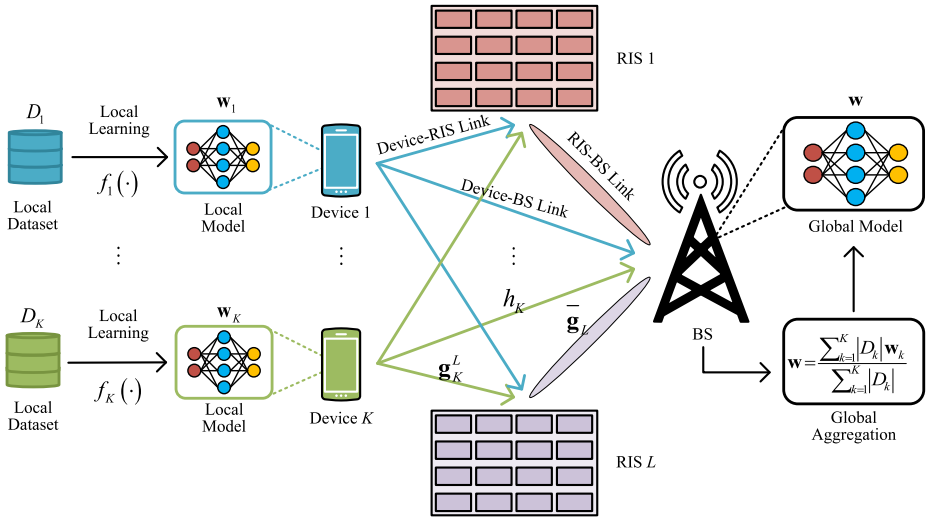

Fig. 1. Illustration of AirFL in multi-RIS-aided IoT networks.

wireless communication systems, including the joint design of active and passive beamforming [21], [32]–[34], the theoretical analysis of fundamental performance limits [35]–[37], as well as the interplay between RIS and other existing technologies, such as mobile-edge computing [38], physical-layer security [39], NOMA [40]–[42], etc. With the objective to maximize the energy efficiency in the RIS-incorporated cellular systems, Huang *et al.* [32] jointly designed the active and passive beamforming in a downlink multiuser communication network. By deploying RISs to eliminate the intercluster interference in MIMO-NOMA networks for performance enhancement, Hou *et al.* [36] obtained the minimal required number of RISs for the signal cancellation demand. Considering the user fairness in RIS-aided systems, the max–min problem was optimized in [33] by designing the transmit power and phase shifts in an iterative manner. Unlike the alternating optimization, to solve the high-dimension problem of the sum-rate maximization in RIS-assisted MIMO systems, Huang *et al.* [34] leveraged the deep reinforcement learning (DRL) to obtain the joint design of the transmit beamforming and the reflection matrix. Similarly, using DRL approaches, an agent for determining the position and phase shifts of RIS was trained in [41] to maximize the long-term energy efficiency of NOMA networks by learning the optimal control strategy in a trial-and-error manner. By leveraging the RIS to mitigate interference in multicell NOMA networks, our prior work in [42] jointly optimized the transmit power, subchannel allocation, reflection matrix, user scheduling, and decoding order to maximize the achievable sum rate. The work in [20] uses multiple RISs to maximize system energy efficiency by dynamically controlling the on–off states of RISs and iteratively optimizing their corresponding phase shifts.

III. System Model

As shown in Fig. 1, we consider a multi-RIS-aided AirFL system consisting of one BS, N IoT devices, and L RISs. Assume that both the BS and devices are equipped with a single antenna, and each RIS comprises M reflecting elements. Instead of aggregating all local model parameters, the number of IoT devices selected to participate in the model uploading process is K out of N ($1 \le K \le N$). The sets of selected devices and RISs are denoted by $\mathcal{K} = \{1, 2, \ldots, K\}$ and $\mathcal{L} = \{1, 2, \ldots, L\}$, respectively. Let $\mathcal{D} = \{\mathcal{D}_1, \mathcal{D}_2, \ldots, \mathcal{D}_K\}$ denote the data set collected by all selected devices, where $\mathcal{D}_k$ is the raw data owned by the kth device. The diagonal matrix of the ℓth RIS is denoted by $\mathbf{\Theta}_\ell = \text{diag}(e^{j\theta_\ell^1}, e^{j\theta_\ell^2}, \ldots, e^{j\theta_\ell^M})$, where $\theta_\ell^m \in [0, 2\pi]$ represents the phase shift of the mth reflecting element at the ℓth RIS.[1]

The block diagram of AirFL[2] is illustrated in Fig. 2, which can be deemed as a function-centric uplink NOMA technique that does not need to decode users' information one by one. All devices transmit their up-to-date local models $\{\mathbf{w}_k | \forall k \in \mathcal{K}\}$ simultaneously over the same time–frequency resource.[3] Then, the nomographic function computed at the BS is given by [28]

$$\psi(\mathbf{w}_1, \mathbf{w}_2, \ldots, \mathbf{w}_K) = \phi\left(\sum_{k=1}^{K} \varphi_k(\mathbf{w}_k)\right) \tag{1}$$

where $\mathbf{w}_k = f_k(\mathcal{D}_k)$ is a parameter vector describing the updated local model weights, and $\varphi_k(\cdot)$ and $\phi(\cdot)$ denote the preprocessing and the post-processing functions at the kth device and the BS, respectively. Before computing the target function $\psi(\cdot)$, the BS needs to collect the target-function

[1] In practice, each RIS can communicate with the BS via a separate link connected by a programmable controller that is capable of smartly adjusting the phase shifts of all reflecting elements in real time [4], [20], [21].

[2] The learning process of AirFL can be easily found in other literature, such as the works in [14], [16], [17], and [29], thus we omit it here for brevity.

[3] Unlike the conventional communicate-then-compute schemes, AirComp is capable of harnessing the channel interference to integrate communication and computation into one concurrent transmission [27]–[29]. Moreover, all selected devices are assumed to be well synchronized so that the signals are perfectly aligned [43]–[45], the analysis of asynchronous transmission is beyond the scope of this article.

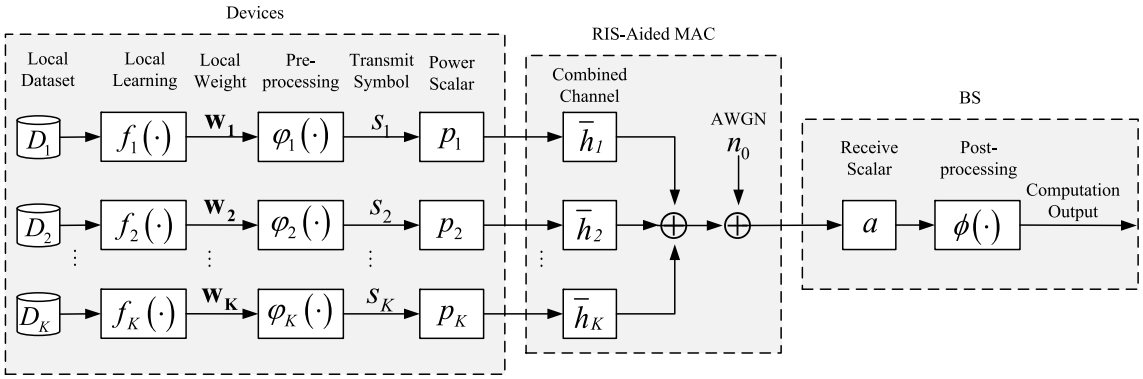

Fig. 2. Block diagram of AirFL in RIS-aided wireless networks.

variable s, denoted by

$$s = \sum_{k=1}^{K} s_k \quad \text{and} \quad s_k = \varphi_k(\mathbf{w}_k) \tag{2}$$

where $s_k \in \mathbb{C}$ is the transmit symbol after preprocessing at the kth device.

Invoking AirComp technique to aggregate distributed model parameters over multi-RIS-aided MAC, the received signal at the BS can be rewritten as

$$y = \sum_{k=1}^{K}\left(h_k + \sum_{\ell=1}^{L} \bar{\mathbf{g}}_\ell \mathbf{\Theta}_\ell \mathbf{g}_k^\ell\right) p_k s_k + n_0 \tag{3}$$

where $h_k \in \mathbb{C}$ denotes the channel response from the kth device to the BS, $\mathbf{g}_k^\ell \in \mathbb{C}^{M\times 1}$ indicates the channel vector from the kth device to the ℓth RIS, and $\bar{\mathbf{g}}_\ell \in \mathbb{C}^{1\times M}$ represents the channel vector from the ℓth RIS to the BS. The scalar $p_k \in \mathbb{C}$ is the transmit power coefficient at the kth device, and n_0 is the additive white Gaussian noise (AWGN) distributed as $\mathcal{CN}(0, \sigma^2)$, while σ^2 is the receive noise power at the BS.

To facilitate analysis and without loss of generality, we assume that the transmit symbols are independent and are normalized with unit variance, i.e., $\mathbb{E}(s_k^H s_{k'}) = 0\ \forall k \neq k'$ and $\mathbb{E}(|s_k|^2) = 1$. Then, the maximum transmit power constraint at the kth device is presented by

$$\mathbb{E}\left(|p_k s_k|^2\right) = |p_k|^2 \leq P_0 \quad \forall k \in \mathcal{K} \tag{4}$$

where $P_0 > 0$ is the transmit power budget at each device.

Upon receiving the analog signal y for computation, the estimation of target variable s is expressed as

$$\hat{s} = \frac{1}{\sqrt{\eta}} a y = \frac{a}{\sqrt{\eta}} \sum_{k=1}^{K} \bar{h}_k p_k s_k + \frac{a}{\sqrt{\eta}} n_0 \tag{5}$$

where $a \in \mathbb{C}$ is a receive scalar employed at the BS. $\bar{h}_k = h_k + \sum_{\ell=1}^{L} \bar{\mathbf{g}}_\ell \mathbf{\Theta}_\ell \mathbf{g}_k^\ell$ refers to the combined channel response, and $\eta > 0$ is a normalizing factor.

Comparing the target-function variable s in (2) with the observed one $\hat{s}$ in (5), the corresponding error can be calculated by $e = \hat{s} - s$. In this article, the MSE is adopted as the performance metric of AirFL, which is different from the rate-centric NOMA transmission in [33], [34], [36], [41], and [42] that aims to maximize the system throughput or the individual rate for the improved spectrum efficiency. Specifically, to quantify the performance of AirFL in global aggregation, the signal distortion of $\hat{s}$ with respect to (w.r.t.) s is measured by the MSE, expressed as

$$\mathrm{MSE}(\hat{s}, s) \triangleq \mathbb{E}\left(|\hat{s} - s|^2\right) = \sum_{k=1}^{K}\left|\frac{1}{\sqrt{\eta}} a \bar{h}_k p_k - 1\right|^2 + \frac{\sigma^2 |a|^2}{\eta}. \tag{6}$$

Note that the first-order Taylor approximation of the computed target function $\hat{\psi} = \phi(\hat{s})$ at s can be rewritten by

$$\hat{\psi} \approx \phi(s) + \phi'(s)(\hat{s} - s). \tag{7}$$

Then, with given $\phi'(s)$, the equivalent transformation between the MSE of ψ and the MSE of s can be expressed as

$$\mathrm{MSE}\left(\hat{\psi}, \psi\right) \approx |\phi'(s)|^2\ \mathrm{MSE}(\hat{s}, s) \tag{8}$$

which implies that a minimum MSE of ψ also leads to a minimum MSE of s. At this point, it can be concluded that the minimization of (6) is a reasonable surrogate of the minimum $\mathrm{MSE}(\hat{\psi}, \psi)$ [46]. Thus, $\mathrm{MSE}(\hat{s}, s)$ is regarded as one of the performance metrics in the rest of this article.

IV. Problem Formulation

Given the considered system model of multi-RIS-aided federated learning, both the aggregation error and convergence rate depend on resource allocation and device selection schemes. Therefore, we shall investigate the optimization of transmit power, receive scalar, reflection coefficients, and learning participants to minimize MSE for prediction accuracy improvement while selecting as more devices as possible for convergence accelerating. To this end, the objective of this work is to minimize the weighted sum of the MSE and cardinality, thus the bicriterion optimization problem can be formulated as

$$(\mathcal{P}0): \min_{\boldsymbol{p}, a, \boldsymbol{\theta}, \mathcal{K}} \quad \mathrm{MSE}(\hat{s}, s) - \gamma|\mathcal{K}| \tag{9a}$$

$$\text{s.t.} \quad |p_k|^2 \leq P_0 \quad \forall k \in \mathcal{K} \tag{9b}$$

$$0 \leq \theta_\ell^m \leq 2\pi \quad \forall \ell, m \tag{9c}$$

$$\mathrm{MSE}(\hat{s}, s) \leq \varepsilon_0 \tag{9d}$$

$$1 \leq |\mathcal{K}| \leq N \tag{9e}$$

where $\boldsymbol{p} = [p_1, p_2, \ldots, p_K]^T$ is the transmit power vector, $\boldsymbol{\theta} = [\theta_1^1, \theta_1^2, \ldots, \theta_1^M, \theta_2^1, \theta_2^2, \ldots, \theta_L^M]^T$ is the phase shift vector, $\varepsilon_0 > 0$ is the aggregation error requirement, $|\mathcal{K}| = K$ is the cardinality of set $\mathcal{K}$, and $\gamma > 0$ is a problem parameter to achieve a tradeoff between the aggregation error and the convergence rate. By adjusting the parameter γ, the optimal tradeoff curve between $\text{MSE}(\hat{s}, s)$ and $|\mathcal{K}|$ can be swept out. Additionally, the transmit power constraints are provided in (9b). The phase shift constraints are given in (9c). The MSE tolerance of global analog aggregation is presented in (9d). The number of learning participants is limited in (9e).

The bicriterion problem (9) is an MINLP problem due to the coupling of continuous variables and discrete variables in both the objective function and constraints. More specifically, the original problem (9) is still intractable even for the case without RISs, i.e., $L = 0$, due to the nonconvex objective function and the combinatorial features of device selection. One can know that it is highly intractable to directly find the global optimal solution of the NP-hard problem (9). Upon this, in order to address this MINLP problem ($\mathcal{P}0$) effectively, we propose to decouple it into two subproblems ($\mathcal{P}1$) and ($\mathcal{P}2$). Specifically, if the set of selected device $\mathcal{K}$ is fixed, problem (9) becomes subproblem (10) of MSE minimization. If the transmit power vector $\boldsymbol{p}$, the receive scalar a and the phase shifts $\boldsymbol{\theta}$ are fixed, problem (9) becomes subproblem (11) of combinatorial optimization.

1) *MSE Minimization*: Given the set of device selection, the first objective is to minimize MSE by dynamically controlling the phase shifts of each RIS and optimizing the transmit power of each selected device as well as the receive scalar at the BS, subject to power constraints for devices and unit-modulus constraints for RISs. As a result, the corresponding MSE minimization subproblem is given by

$$(\mathcal{P}1): \min_{\boldsymbol{p},a,\boldsymbol{\theta}} \ \text{MSE}\big(\hat{s}, s\big) \tag{10a}$$

$$\text{s.t.} \ \ (9b) \ \ \text{and} \ \ (9c). \tag{10b}$$

2) *Combinatorial Optimization*: Given the transceiver design and the reflection vector, the second objective is to minimize the aggregation error and maximize the number of selected devices at the same time by solving the following combinatorial optimization subproblem, subject to the MSE requirement for global aggregation and the cardinality constraint for participant number, which can be formulated as

$$(\mathcal{P}2): \min_{\mathcal{K}} \ \text{MSE}\big(\hat{s}, s\big) - \gamma|\mathcal{K}| \tag{11a}$$

$$\text{s.t.} \ \ (9d) \ \ \text{and} \ \ (9e). \tag{11b}$$

The MSE minimization problem (10) is nonlinear and nonconvex even for the single-device case with $K = 1$, due to the close coupling of $\boldsymbol{p}$, a, and $\boldsymbol{\theta}$ in $\text{MSE}(\hat{s}, s)$. Not to mention that problem (10) is still nonconvex even when we only check the feasibility of phase shifts design. Moreover, the combinatorial optimization problem (11) with multiple constraints is NP-hard and is nontrivial to obtain a high-performance solution as well. Furthermore, problem (10) is still a challenging issue even when some simplified cases are considered, while it is also almost impossible to obtain a closed-form solution to problem (11). Fortunately, some common relaxation approaches can be adopted to transform the nonconvex subproblems into convex ones, which can be solved separately and alternatively over iterations. This motivates us to decompose the original problem into multiple subproblems. Thus, an intuitive approach is to adopt the alternating optimization technique for solving the nonlinear and nonconvex problem (9) in an efficient manner, i.e., only optimize one variable in a single step, then repeat this over all variables in turn until the termination condition is satisfied.

However, due to the rapidly varying CSI, it is impractical and not cost effective for the resource-scarce devices to acquire global CSI when they allocate transmit power for model uploading. To reduce the high signaling overhead of CSI feedback, it is of significance to develop a communication-efficient scheme for distributed power allocation. Furthermore, one straightforward approach to find the optimal set of participating devices is the exhaustive search, but it inevitably results in an unacceptable computational complexity, i.e., $\mathcal{O}(2^N)$. As a result, to avoid the exponential complexity, it is imperative and desirable to design computation-efficient algorithms with polynomial time complexity.

To illustrate the problem decomposition, we provide a tree diagram in Fig. 3 to clearly delineate the connections between the key reformulated subproblems and the corresponding solutions. Specifically, when the set of selected devices is fixed, the nonconvex MSE minimization subproblem (10) is solved by the derived closed-form solutions and the developed SCA-based algorithm. When the transceiver and reflection coefficients are fixed, finding the optimal solution is still nontrivial due to the combinatorial property of subproblem (11) in terms of the device selection. Inspired by the DC representation method described in [47], a natural way to address it is invoking the DC programming. Additionally, we provide a flowchart in Fig. 4 to draw the steps of the proposed alternating optimization algorithm for solving resource allocation and device selection problems in single-antenna cases. The flowchart for multiantenna cases can be obtained similarly. Our specific solutions to subproblems in terms of transmit power, receive scalar, phase shifts, and device selection are presented in Section V.

V. Alternating Optimization

A. Transmit Power Allocation

Using the channel estimation approaches designed in [48] and [49], the global CSI is assumed to be available at the BS, while each local device only knows the receive scalar a as well as its own CSI. Furthermore, given the vector of phase shifts $\boldsymbol{\theta}$ in subproblem (10), the optimal transmit power at the kth device can be derived in closed form. Specifically, through minimizing $\text{MSE}(\hat{s}, s)$ in the objective function (10a), we have $\sum_{k=1}^{K} |a\bar{h}_k p_k/\sqrt{\eta} - 1|^2 = 0$. Then, the optimal transmit power at the kth device is given by

$$p_k^* = \sqrt{\eta}\frac{\big(a\bar{h}_k\big)^H}{\big|a\bar{h}_k\big|^2} \quad \forall k \in \mathcal{K} \tag{12}$$

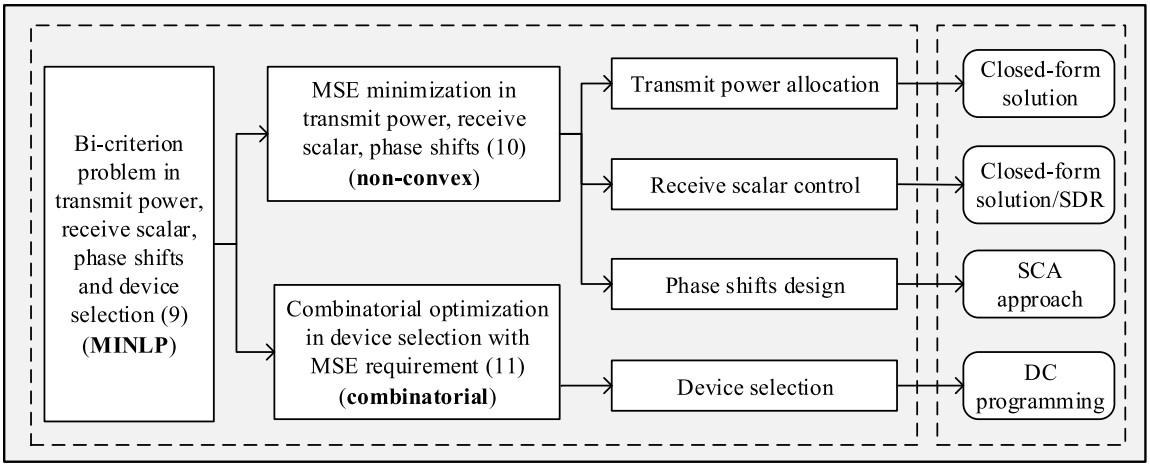

Fig. 3. Overview of the problem decomposition and proposed methods to subproblems.

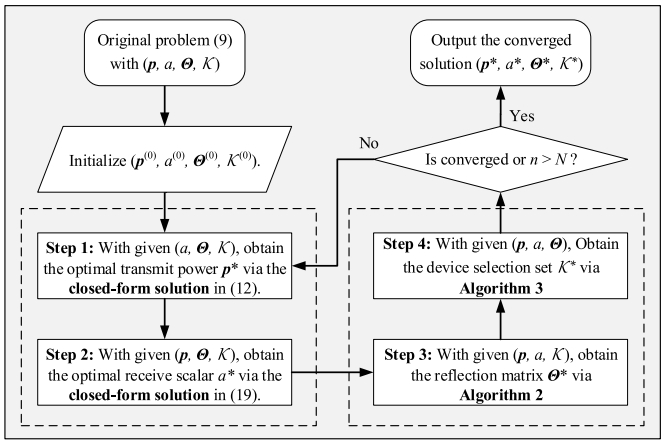

Fig. 4. Flowchart of the proposed alternating optimization algorithm.

where the channel condition $\bar{h}_k$ in (12) can be further tuned by the multiple geodistributed RISs, thereby reducing the energy consumption of transmitters and prolonging network lifetime.

Combining the transmit power constraints for all devices in (9b), the normalizing factor η employed at the BS can be obtained by

$$\eta = P_0 \min_k \left|a\bar{h}_k\right|^2 \tag{13}$$

which is determined by the transmit power budget P_0 and the minimum combined channel gain $|\bar{h}_k|^2$ among all devices as well as the receive scalar a at the BS. Hence, one can see from (12) that the optimal transmit power p_k^* at the kth device only depends on its own CSI $\bar{h}_k$, while other parameters, such as η and a, are directly obtained from the BS in a broadcasting manner. This is conducive to the implementation of semidistributed power control, thus further saving system bandwidth and mitigating traffic congestion in resource-scarce IoT networks. More specifically, the individual cascaded CSI $\bar{h}_k$ at the kth device can be effectively estimated from the downlink multicasting pilot signals.

Combining (12) and (13), the MSE measurement in (6) is further rewritten as

$$\mathrm{MSE}(\hat{s}, s) = \frac{\sigma^2|a|^2}{P_0 \min_k \left|a\bar{h}_k\right|^2}. \tag{14}$$

Then, the MSE minimization problem (10) can be reformulated as

$$\min_{a,\boldsymbol{\theta}} \ \max_k \frac{\sigma^2|a|^2}{P_0\left|a\bar{h}_k\right|^2} \quad \text{s.t. (9c).} \tag{15}$$

Proposition 1: When the BS is equipped with N_r antennas, the receive vector can be denoted by $\boldsymbol{a} \in \mathbb{C}^{N_r \times 1}$ and the combined channel vector becomes $\bar{\boldsymbol{h}}_k \in \mathbb{C}^{N_r \times 1}$. Then, similar to the solutions obtained in (12), the optimal transmit power at the kth device and the normalizing factor at the BS can be derived as

$$p_k^* = \sqrt{\eta}\frac{\left(\boldsymbol{a}^H\bar{\boldsymbol{h}}_k\right)^H}{\left\|\boldsymbol{a}^H\bar{\boldsymbol{h}}_k\right\|^2} \quad \forall k \in \mathcal{K} \tag{16}$$

$$\eta = P_0 \min_k \left\|\boldsymbol{a}^H\bar{\boldsymbol{h}}_k\right\|^2 \tag{17}$$

where $\bar{\boldsymbol{h}}_k = \boldsymbol{h}_k + \sum_{\ell=1}^{L} \bar{\boldsymbol{G}}_\ell \boldsymbol{\Theta}_\ell \boldsymbol{g}_k^\ell$, $\boldsymbol{h}_k \in \mathbb{C}^{N_r \times 1}$ is the channel vector between the BS and the kth device, and $\bar{\boldsymbol{G}}_\ell \in \mathbb{C}^{N_r \times M}$ is the channel matrix from the ℓth RIS to the BS.

B. Receive Scalar Control

To effectively solve the min–max problem (15) of joint reflection and receive, we reformulate it into a minimization problem with nonconvex quadratic constraints, i.e.,

$$\min_{a,\boldsymbol{\theta}} \ |a|^2 \tag{18a}$$

$$\text{s.t.} \ \left|a\bar{h}_k\right|^2 \geq 1 \quad \forall k \in \mathcal{K} \tag{18b}$$

$$\text{(9c).} \tag{18c}$$

Next, the closed-form solutions are provided for the optimal design of receive scalar and reflection matrix.

Theorem 1: The optimal receive scalar a^* to problem (18) can be given by

$$\left|a^*\right| = \frac{1}{\min_k \left|\bar{h}_k\right|}. \tag{19}$$

Meanwhile, the optimal reflection matrix $\mathbf{\Theta}_\ell^*$ satisfies

$$\arg\left(\sum_{\ell=1}^{L} \bar{\mathbf{g}}_\ell \mathbf{\Theta}_\ell^* \mathbf{g}_k^\ell\right) = \arg(h_k) \quad \forall k \in \mathcal{K} \tag{20}$$

where $\arg(\cdot)$ is a function that returns the phase shift of the input complex number.

Proof: See Appendix A. ∎

It can be noticed that the objective value of problem (18) just depends on the amplitude of the receive scalar a, we thus only need to optimize $|a|$ and the phase shift of a can be arbitrary, which is confirmed by the closed-form solution (19) obtained in Theorem 1. Furthermore, due to the implicit expression in (20), one can know that the optimal reflection matrix $\mathbf{\Theta}_\ell^*$ is not unique, the approach to find a feasible one will be proposed in Section V-C. As an extension, the receiving control problem in the multiantenna case at the BS is given as follows.

Corollary 1: Considering the multiantenna case with the solutions derived in Proposition 1, the problem (18) in the multiantenna case can be rewritten as

$$\min_{\boldsymbol{a},\boldsymbol{\theta}} \ \|\boldsymbol{a}\|^2 \tag{21a}$$

$$\text{s.t.} \ \left\|\boldsymbol{a}^H \bar{\boldsymbol{h}}_k\right\|^2 \geq 1 \quad \forall k \in \mathcal{K} \tag{21b}$$

$$\text{(9c)}. \tag{21c}$$

According to problem (21) in Corollary 1, when the phase shifts $\boldsymbol{\theta}$ are fixed, the subproblem of receive vector control in the multiantenna case is given by

$$\min_{\boldsymbol{a}} \|\boldsymbol{a}\|^2 \quad \text{s.t. (21b)}. \tag{22}$$

To address the nonconvexity of problem (22), the matrix lifting technique is invoked as an intuitive method to rewrite it as a semidefinite programming (SDP) problem. Specifically, we first introduce auxiliary variables $\mathbf{H}_k = \bar{\boldsymbol{h}}_k \bar{\boldsymbol{h}}_k^H$ and $\mathbf{A} = \boldsymbol{a}\boldsymbol{a}^H$ while satisfying $\mathbf{A} \succeq \mathbf{0}$ and $\text{rank}(\mathbf{A}) = 1$. Then, problem (22) can be shown to be equivalent to the following problem (23) with a nonconvex rank-one constraint:

$$\min_{\mathbf{A}} \ \text{tr}(\mathbf{A}) \tag{23a}$$

$$\text{s.t.} \ \text{tr}(\mathbf{A}\mathbf{H}_k) \geq 1 \quad \forall k \in \mathcal{K} \tag{23b}$$

$$\mathbf{A} \succeq \mathbf{0} \tag{23c}$$

$$\text{rank}(\mathbf{A}) = 1. \tag{23d}$$

Thereby, the SDR technique can be applied to find an upper bound for the optimal solution of problem (23). The rank-one constraint (23d) is simply omitted to relax problem (23) into a convex one, given by

$$\min_{\mathbf{A}} \ \text{tr}(\mathbf{A}) \tag{24a}$$

$$\text{s.t.} \ \text{(23b)} \ \text{and} \ \text{(23c)}. \tag{24b}$$

Since the only nonconvex constraint of $\text{rank}(\mathbf{A}) = 1$ is dropped, the resulting problem (23) can be efficiently solved by off-the-shelf optimization toolkits such as CVX [50]. We can recover the optimal receive scaling vector $\boldsymbol{a}^*$ by using the rank-one decomposition $\mathbf{A}^* = \boldsymbol{a}^* \boldsymbol{a}^{*\mathrm{H}}$, if the obtained optimal solution $\mathbf{A}^*$ satisfies $\text{rank}(\mathbf{A}^*) = 1$. Otherwise, when $\text{rank}(\mathbf{A}^*) \neq 1$, through calculating the maximum eigenvalue λ and the eigenvector $\mathbf{u}$ via $\tilde{\mathbf{A}}^* = \lambda \mathbf{u}\mathbf{u}^H$, a suboptimal rank-one solution can be obtained to approximate the optimal solution $\mathbf{A}^*$. In this way, a suboptimal receive scaling vector $\tilde{\boldsymbol{a}}^*$ can be approximately calculated by $\tilde{\boldsymbol{a}}^* = \sqrt{\lambda}\mathbf{u}$. As a surrogate approach, if the obtained solution $\mathbf{A}^*$ fails to be rank-one, the Gaussian randomization method [42], [51] can be invoked to find a feasible solution to problem (23).

Note that dropping the rank-one constraint directly also brings limitations such as performance loss, especially when the SDR is not tight for problem (23). To this end, the SCA method is adopted in the following to solve problem (22) in an efficient manner. First, some auxiliary variables are introduced to represent the real part and the imaginary part of $\boldsymbol{a}^H \bar{\boldsymbol{h}}_k$, which is given by

$$\mathbf{b}_k = \left[\bar{x}_k, \ \bar{y}_k\right]^T \quad \forall k \in \mathcal{K} \tag{25}$$

where $\bar{x}_k = \text{Re}(\boldsymbol{a}^H \bar{\boldsymbol{h}}_k)$, $\bar{y}_k = \text{Im}(\boldsymbol{a}^H \bar{\boldsymbol{h}}_k)$. Then, the nonconvex constraint (21b) becomes $\|\boldsymbol{a}^H \bar{\boldsymbol{h}}_k\|^2 = \|\mathbf{b}_k\|^2 \geq 1 \ \forall k \in \mathcal{K}$, which is still nonconvex [46]. To solve problem (21) with the SCA method, the first-order Taylor expansion is adopted to obtain the lower bound of the nonconvex part based on the previous iteration, i.e.,

$$\|\mathbf{b}_k\|^2 \geq \left\|\mathbf{b}_k^{(z)}\right\|^2 + 2\left(\mathbf{b}_k^{(z)}\right)^T \left(\mathbf{b}_k - \mathbf{b}_k^{(z)}\right) \geq 1 \quad \forall k \in \mathcal{K} \tag{26}$$

where $\mathbf{b}_k^{(z)}$ is the solution obtained at the zth iteration.

Thus, with the help of the auxiliary variables defined in (25), the nonconvex constraint (21b) can be replaced with its approximation (26) at each iteration. Then, problem (22) can be transformed into the following tractable form:

$$\min_{\boldsymbol{a},\{\mathbf{b}_k\}} \ \|\boldsymbol{a}\|^2 \quad \text{s.t. (25)} \ \text{and (26)} \tag{27}$$

which is convex and can be efficiently solved by CVX as well. Specifically, we first solve problem (24) to obtain an initial solution of $\boldsymbol{a}^{(0)}$ and $\{\mathbf{b}_k^{(0)}\}$. Then, the achievable performance can be continuously improved by solving problem (27) in an iterative fashion. Thus, based on the above analysis for the multiantenna case at the BS, the SDR-based algorithm for receive vector control can be summarized in Algorithm 1.

C. Phase Shifts Design

Although the implicit expression of the optimal reflection matrix has been given in (20), it is still difficult to search an optimal solution due to its nonuniqueness and the curse of dimensionality. Therefore, it is necessary to develop an efficient method to solve the problem of phase shifts design suboptimally. Specifically, given the receive scalar a, the problem (18) is reduced to a feasibility-check problem and can be reformulated as

$$\text{find} \ \ \boldsymbol{\theta} \tag{28a}$$

$$\text{s.t.} \ \text{(9c)} \ \text{and} \ \text{(18b)}. \tag{28b}$$

Algorithm 1 SDR-Based Algorithm for Receiving Control

Initialize the accuracy ϵ, the maximum iteration number N_1, and the current iteration index $n_1 = 0$.
Given $\boldsymbol{p}$ and $\boldsymbol{\theta}$, compute $\mathbf{A}^*$ by solving (24).
if $\text{rank}(\mathbf{A}^*) = 1$ **then**
  Recover $\boldsymbol{a}^*$ by calculating $\mathbf{A}^* = \boldsymbol{a}^*\boldsymbol{a}^{*\text{H}}$.
else
  Compute the eigen-decomposition $\tilde{\mathbf{A}}^* = \lambda \mathbf{u}\mathbf{u}^{\text{H}}$.
  Obtain $\boldsymbol{a}^{(0)} = \tilde{\boldsymbol{a}}^* = \sqrt{\lambda}\mathbf{u}$.
  Derive $\{\mathbf{b}_k^{(0)}\} = \left\{\left[\text{Re}(\tilde{\boldsymbol{a}}^{*\text{H}}\bar{\boldsymbol{h}}_k), \text{Im}(\tilde{\boldsymbol{a}}^{*\text{H}}\bar{\boldsymbol{h}}_k)\right] | \forall k\right\}$.
  repeat
    Compute $\boldsymbol{a}^{(n_1+1)}$ and $\{\mathbf{b}_k^{(n_1+1)}\}$ by solving (27).
    Update $n_1 \coloneqq n_1 + 1$.
  until $|\boldsymbol{a}^{(n_1)} - \boldsymbol{a}^{(n_1-1)}|^2 < \epsilon$ or $n_1 > N_1$.
end if
Output the optimal $\boldsymbol{a}^*$ or the converged solution $\boldsymbol{a}^{(n_1)}$.

Since only a feasible solution of the phase shifts $\boldsymbol{\theta}$ can be obtained by solving problem (28), it remains unknown whether the objective value of (18) will monotonically decrease or not over iterations. From the closed-form solution obtained in (19), one can know that the value of $\min_k |\bar{h}_k|$ should be maximized to enforce the reduction of the receive scalar $|a|$ over iterations. To this end, we transform the above feasibility-check problem (28) into a max–min problem with an explicit objective to enforce the reduction of $|a|$ for achieving better performance and faster convergence. As a result, the problem (28) is rewritten as

$$\max_{\boldsymbol{\theta}} \ \min_{k\in\mathcal{K}} \ \left|\bar{h}_k\right| \quad \text{s.t. (9c).} \tag{29}$$

Then, we introduce an auxiliary variable $\beta = \min_{k\in\mathcal{K}} \ |\bar{h}_k|$ to further transform the max–min problem (29) into a joint maximization problem w.r.t. $\boldsymbol{\theta}$ and β, which is given by

$$\max_{\boldsymbol{\theta},\beta} \ \beta \tag{30a}$$

$$\text{s.t.} \ \left|\bar{h}_k\right|^2 \geq \beta \quad \forall k \in \mathcal{K}, \tag{30b}$$

$$\text{(9c)}. \tag{30c}$$

It is obvious that both the objective and constraints are linear functions for β, but the quadratically constraint (30b) is nonconvex for $\boldsymbol{\theta}$. Additionally, due to the uncertainty of phase rotation [21], the problem (30) cannot be straightforwardly transformed into a tractable second-order cone programming (SOCP) optimization problem. Therefore, we combine the penalty method and SCA technique to approximately solve it in the following content.

Let $v_\ell^m = e^{j\theta_\ell^m}$, then the equivalent channel fading after receiver scaling w.r.t. the ℓth RIS for the kth device can be denoted as

$$\bar{\mathbf{g}}_\ell \boldsymbol{\Theta}_\ell \mathbf{g}_k^\ell = \boldsymbol{\Phi}_k^\ell \mathbf{v}_\ell \tag{31}$$

where $\mathbf{v}_\ell = [e^{j\theta_\ell^1}, e^{j\theta_\ell^2}, \ldots, e^{j\theta_\ell^M}]^T$ and $\boldsymbol{\Phi}_k^\ell = \bar{\mathbf{g}}_\ell \text{diag}(\mathbf{g}_k^\ell)$.

As such, constraint (30b) is transformed as

$$\left|h_k + \sum_{\ell=1}^{L} \bar{\mathbf{g}}_\ell \boldsymbol{\Theta}_\ell \mathbf{g}_k^\ell\right|^2 = \left|h_k + \sum_{\ell=1}^{L} \boldsymbol{\Phi}_k^\ell \mathbf{v}_\ell\right|^2 \geq \beta \quad \forall k. \tag{32}$$

With the above substitutions (32), the joint maximization problem (30) can be rewritten as

$$\max_{\mathbf{v},\beta} \ \beta \tag{33a}$$

$$\text{s.t.} \ \left|v_\ell^m\right| = 1 \quad \forall \ell, m \tag{33b}$$

$$|h_k + \boldsymbol{\Phi}_k \mathbf{v}|^2 \geq \beta \quad \forall k \tag{33c}$$

where $\mathbf{v} = [\mathbf{v}_1, \mathbf{v}_2, \ldots, \mathbf{v}_L]^H$ and $\boldsymbol{\Phi}_k = [\boldsymbol{\Phi}_k^1, \boldsymbol{\Phi}_k^2, \ldots, \boldsymbol{\Phi}_k^L]$. Although the variables and constraints in (33) have changed and are different from those in (30), it is still intractable to solve problem (33) directly and optimally on account of the nonconvex constraints (33b) and (33c).

To transform constraint (33b) into a more tractable form, through introducing a positive penalty parameter $\zeta > 0$, the penalty function method is adopted to reformulate problem (33), which is given by

$$\max_{\mathbf{v},\beta} \ \beta + \zeta \sum_{\ell=1}^{L}\sum_{m=1}^{M}\left(\left|v_\ell^m\right|^2 - 1\right) \tag{34a}$$

$$\text{s.t.} \ \left|v_\ell^m\right| \leq 1 \quad \forall \ell, m, \tag{34b}$$

$$\text{(33c)}. \tag{34c}$$

It can be observed that if the punished component $(|v_\ell^m|^2 - 1)$ in the objective function (34a) is enforced to be zero as the search proceeds, then we can obtain an optimal solution to problem (34). Otherwise, we can claim that the current solution is likely to be further improved over iterations.

Next, in order to tackle the nonconvex objective function (34a), we apply the common SCA method to approximate it as $\beta + 2\zeta \sum_{\ell=1}^{L}\sum_{m=1}^{M} \text{Re}((v_\ell^{m(z)})^H(v_\ell^m - v_\ell^{m(z)}))$, where $v_\ell^{m(z)}$ is obtained at the zth iteration. Likewise, we use the first-order Taylor expansion to deal with the nonconvex constraint (33c), which can be expressed as

$$|h_k + \boldsymbol{\Phi}_k \mathbf{v}|^2 \geq 2\text{Re}\left(\left(h_k + \boldsymbol{\Phi}_k \mathbf{v}^{(z)}\right)^H \boldsymbol{\Phi}_k\left(\mathbf{v} - \mathbf{v}^{(z)}\right)\right) + \left|h_k + \boldsymbol{\Phi}_k \mathbf{v}^{(z)}\right|^2 \geq \beta \quad \forall k \in \mathcal{K} \tag{35}$$

where $\mathbf{v}^{(z)}$ is the converged value at the zth iteration.

Consequently, replacing the intractable parts (34a) and (33c) with their approximations given above, the nonconvex problem (34) is approximated by

$$\max_{\mathbf{v},\beta} \ \beta + 2\zeta \sum_{\ell=1}^{L}\sum_{m=1}^{M} \text{Re}\left(\left(v_\ell^{m(z)}\right)^H\left(v_\ell^m - v_\ell^{m(z)}\right)\right) \tag{36a}$$

$$\text{s.t.} \ \text{(34b)} \ \text{and} \ \text{(35)}. \tag{36b}$$

Since the objective function (36a) is linear and the feasible set with constraint (36b) is convex, problem (36) is a jointly convex optimization problem w.r.t. variables $\mathbf{v}$ and β. The details of using the SCA method to solve problem (36) at each iteration are summarized in Algorithm 2. Analogous to the previous analysis, the developed SCA-based algorithm can be extended to the multiantenna case without much effort, thus the details are omitted here for brevity.

Algorithm 2 SCA-Based Algorithm for Phase Shifts Design

1: **Initialize** $\mathbf{v}^{(0)}$, $\beta^{(0)}$, the tolerances ϵ_1 and ϵ_2, the maximum iteration number N_2, and set the current iteration number as $n_2 = 1$.
2: **repeat**
3: Compute $(\mathbf{v}^{(n_2)}, \beta^{(n_2)})$ by solving problem (36).
4: Calculate $\delta_1 = 2\zeta \sum_\ell \sum_m \mathrm{Re}((v_\ell^{m(n_2-1)})^{\mathrm{H}}(v_\ell^{m(n_2)} - v_\ell^{m(n_2-1)}))$.
5: Calculate $\delta_2 = \beta^{(n_2)} - \beta^{(n_2-1)}$.
6: Update $n_2 := n_2 + 1$.
7: **until** $(\delta_1^2 \le \epsilon_1$ and $\delta_2^2 \le \epsilon_2)$ or $n_2 > N_2$.
8: **Output** the converged solutions $\mathbf{v}^{(n_2)}$ and $\beta^{(n_2)}$.

D. Device Selection

Substituting (14) into (11), the combinatorial optimization problem w.r.t. device selection is rewritten as

$$\min_{\mathcal{K}} \ \frac{\sigma^2|a|^2}{P_0 \min_k \left|a\bar{h}_k\right|^2} - \gamma|\mathcal{K}| \tag{37a}$$

$$\text{s.t.} \ \ |a|^2 - \rho\left|a\bar{h}_k\right|^2 \le 0 \quad \forall k \in \mathcal{K} \tag{37b}$$

$$1 \le |\mathcal{K}| \le N \tag{37c}$$

where $\rho = \varepsilon_0 P_0/\sigma^2$ is a constant.

The objective function (37a) is not only related to the set cardinality $|\mathcal{K}|$ but also depends on the minimum equivalent channel gain. Thus, solving this minimization problem (37) is highly intractable as it requires a complex combinatorial optimization where the elements in $\mathcal{K}$ directly affect both the value of $\min_k |a\bar{h}_k|^2$ and the number of feasible constraints (37b). To support efficient algorithm design, we propose to reformulate the problem (37) as a joint optimization problem presented in the following lemma.

Lemma 1: Let $\tau = (\bar{\rho}/[\min_k |a\bar{h}_k|^2])$, where $\bar{\rho} = ([\sigma^2|a|^2]/\gamma P_0)$. Then, the problem (37) can be equivalently transformed into the following joint maximization problem:

$$\max_{\mathcal{K},\tau} \ |\mathcal{K}| - \tau \tag{38a}$$

$$\text{s.t.} \ \ \bar{\rho} - \tau\left|a\bar{h}_k\right|^2 \le 0 \quad \forall k \in \mathcal{K} \tag{38b}$$

$$1 - \rho\left|\bar{h}_k\right|^2 \le 0 \quad \forall k \in \mathcal{K} \tag{38c}$$

$$1 \le |\mathcal{K}| \le N. \tag{38d}$$

Proof: See Appendix B. ∎

Note that a tradeoff relationship between $|\mathcal{K}|$ and τ is formed in problem (38). Specifically, if the number of feasible constraints is increased (i.e., a larger $|\mathcal{K}|$), then the value of τ in (38b) shall be larger as well, which may make the objective value decrease and vice versa. To solve this nontrivial problem, we first introduce an auxiliary vector $\boldsymbol{e} = [e_1, e_2, \ldots, e_N] \in \mathbb{R}_+^N$, then the problem (37) can be equivalently reformulated as

$$\min_{\boldsymbol{e}\in\mathbb{R}_+^N,\tau} \ \|\boldsymbol{e}\|_0 + \tau \tag{39a}$$

$$\text{s.t.} \quad \bar{\rho} - \tau\left|a\bar{h}_k\right|^2 \le e_k \quad \forall k \in \mathcal{K} \tag{39b}$$

$$1 - \rho\left|\bar{h}_k\right|^2 \le e_k \quad \forall k \in \mathcal{K} \tag{39c}$$

$$1 \le |\mathcal{K}| \le N \tag{39d}$$

where $\|\boldsymbol{e}\|_0$ is the ℓ_0 norm and is equal to the number of nonzero elements in $\boldsymbol{e}$, and $\mathbb{R}_+^N$ denotes the nonnegative space of $1 \times N$ real-valued vector

Thus, it can be known from (39) that the nth device should be selected to participate in the model uploading process if $e_n = 0, n = 1, \ldots, N$. To handle the nonconvexity of (39a), the ℓ_0 norm can be rewritten as the difference of two convex functions, which is given by [47]

$$\|\boldsymbol{e}\|_0 = \min\{k : \|\boldsymbol{e}\|_1 - |||\boldsymbol{e}|||_k = 0, \ 0 \le k \le N\} \tag{40}$$

where $\|\boldsymbol{e}\|_1$ is the ℓ_1 norm and is calculated by the sum of all absolute values, and $|||\boldsymbol{e}|||_k$ is the Ky Fan k norm and is obtained by the sum of largest-k absolute values.

Replacing (39a) with (40), problem (39) is expressed as the DC programming problem

$$\min_{\boldsymbol{e},\tau} \ \|\boldsymbol{e}\|_1 + \tau - |||\boldsymbol{e}|||_k \tag{41a}$$

$$\text{s.t.} \ \ (39\text{b}) \ \text{and} \ (39\text{c}) \tag{41b}$$

$$\boldsymbol{e} \succeq \mathbf{0} \tag{41c}$$

where $\boldsymbol{e} \succeq \mathbf{0}$ denotes that all elements in vector $\boldsymbol{e}$ are greater than or equal to zero.

Although problem (41) is nonconvex, it can be solved by the majorization–minimization algorithm [52] in an iterative fashion. To ensure a convergent solution, we add quadratic terms to make both $\tilde{g}$ and $\tilde{h}$ be α-strongly convex functions. Meanwhile, the indicator function $I(\boldsymbol{e})$ can be denoted by

$$I(\boldsymbol{e}) = \begin{cases} 0, & \text{if } \boldsymbol{e} \succeq \mathbf{0} \\ +\infty, & \text{otherwise.} \end{cases} \tag{42}$$

Then, the DC objective (41a) is rewritten as the difference of two strongly convex functions, i.e., $\tilde{g} - \tilde{h}$, which can be given by

$$\tilde{f} = \tilde{g} - \tilde{h} = \|\boldsymbol{e}\|_1 + \tau - |||\boldsymbol{e}|||_k + I(\boldsymbol{e}) \tag{43}$$

where $\tilde{g} = \|\boldsymbol{e}\|_1 + \tau + (\alpha/2)\|\boldsymbol{e}\|_F^2 + I(\boldsymbol{e})$ and $\tilde{h} = |||\boldsymbol{e}|||_k + (\alpha/2)\|\boldsymbol{e}\|_F^2$.

By replacing the nonconvex part $\tilde{h}$ with its linear approximation, problem (41) can be reconstructed as the following jointly convex optimization problem:

$$\min_{\boldsymbol{e},\tau} \ \tilde{g} - \langle \partial_{\boldsymbol{e}^{(z)}}\tilde{h}, \boldsymbol{e}\rangle \tag{44a}$$

$$\text{s.t.} \ \ (39\text{b}), (39\text{c}), \text{and} \ (41\text{c}) \tag{44b}$$

where $\boldsymbol{e}^{(z)}$ is the obtained solution at the zth iteration, $\partial_{\boldsymbol{e}^{(z)}}\tilde{h}$ is the subgradient of $\tilde{h}$ w.r.t. $\boldsymbol{e}$ at $\boldsymbol{e}^{(z)}$, and $\langle \partial_{\boldsymbol{e}^{(z)}}\tilde{h}, \boldsymbol{e}\rangle$ denotes the inner product of two vectors. Specifically, the subgradient of $\tilde{h}$ w.r.t. $\boldsymbol{e}$ can be given by

$$\partial_{\boldsymbol{e}}\tilde{h} = \partial|||\boldsymbol{e}|||_k + \alpha\boldsymbol{e} \tag{45}$$

where the nth entry of $\partial|||\boldsymbol{e}|||_k$ can be computed by

$$\partial|||\boldsymbol{e}|||_k = \begin{cases} \mathrm{sign}(e_n), & |e_n| \ge |e_{(k)}| \\ 0, & |e_n| < |e_{(k)}|. \end{cases} \tag{46}$$

The proposed DC-based algorithm for solving problem (44) is summarized in Algorithm 3. Additionally, the process of using DC programming to solve the device selection problem in the multiantenna case at the BS can be developed similarly,

Algorithm 3 DC-Based Algorithm for Device Selection

1: **Initialize** $\boldsymbol{e}^{(0)}$, $\tau^{(0)}$, the tolerance ϵ, the maximum iteration number N_3, and set $n_3 = 0$.
2: **repeat**
3: Calculate the subgradient $\partial_{\boldsymbol{e}^{(n_3)}}\tilde{h}$.
4: Compute the inner product $\langle \partial_{\boldsymbol{e}^{(n_3)}}\tilde{h}, \boldsymbol{e}\rangle$.
5: Obtain $(\boldsymbol{e}^{(n_3+1)}, \tau^{(n_3+1)})$ by solving problem (44).
6: Update $n_3 := n_3 + 1$;
7: **until** the decrease value of (44a) is below ϵ or $n_3 > N_3$.
8: **Output** the converged solution $(\boldsymbol{e}^{(n_3)}, \tau^{(n_3)})$.

Algorithm 4 Alternating Optimization Algorithm for Solving Problem (9)

1: **Initialize** a feasible solution $(\boldsymbol{p}^{(0)}, a^{(0)}, \boldsymbol{v}^{(0)}, \boldsymbol{e}^{(0)})$, the maximum iteration number is denoted by N_4, and set the current iteration number as $n_4 = 0$.
2: **repeat**
3: **Step 1:** transmit power allocation
4: Given $(a^{(n_4)}, \boldsymbol{v}^{(n_4)}, \boldsymbol{e}^{(n_4)})$, obtain the transmit power $\boldsymbol{p}^{(n_4+1)}$ and normalizing factor $\eta^{(n_4+1)}$ by using the closed-form expressions in (12) and (13).
5: **Step 2:** receive scalar control
6: Given $(\boldsymbol{p}^{(n_4+1)}, \boldsymbol{v}^{(n_4)}, \boldsymbol{e}^{(n_4)})$, calculate scalar $a^{(n_4+1)}$ by using the closed-form solution derived in (19).
7: **Step 3:** phase shifts design
8: Given $(\boldsymbol{p}^{(n_4+1)}, a^{(n_4+1)}, \boldsymbol{e}^{(n_4)})$, solve the reflection design subproblem (36) to obtain $\boldsymbol{v}^{(n_4+1)}$ by using Algorithm 2.
9: **Step 4:** device selection
10: Given $(\boldsymbol{p}^{(n_4+1)}, a^{(n_4+1)}, \boldsymbol{v}^{(n_4+1)})$, solve the device selection subproblem (44) to obtain $\boldsymbol{e}^{(n_4+1)}$ by using Algorithm 3.
11: Update $n_4 := n_4 + 1$.
12: **until** the objective value of (9) converges or $n_4 > N_4$.
13: **Output** the converged solution $(\boldsymbol{p}^{(n_4)}, a^{(n_4)}, \boldsymbol{v}^{(n_4)}, \boldsymbol{e}^{(n_4)})$.

which is omitted here for brevity. Till now, one can see that the decoupled subproblems have been transformed into the solvable range of existing optimization toolkits one by one.

E. Convergence and Complexity

According to the derived closed-form solutions and the developed iterative algorithms in the previous sections, an alternating optimization algorithm is proposed to solve the original challenging problem (9). The overall algorithm framework for dealing with the single-antenna case is given in Algorithm 4. According to the closed-form solutions of the transceiver design derived in (12) and (13), the first step of Algorithm 4 is to allocate the transmit power at devices and tune the normalizing factor at the BS. Then, with the optimal design of receive scalar obtained in (19), the second step of Algorithm 4 is to control the scaling factor employed at the BS. Next, using the converged solutions output by Algorithm 2, the third step of Algorithm 4 is to adjust the reflection matrix at each RIS. In the fourth step, the devices participating in the model updating process are selected by the BS based on the DC algorithm, i.e., Algorithm 3. Previously, a holistic flowchart of our designed alternating optimization algorithm has been given in Fig. 4. In addition, the alternating optimization algorithm for solving the problems in the multiantenna case is analogous to the processes of Algorithm 4, the main differences are: 1) replacing the closed-form expressions (12) and (13) with the solutions obtained in Proposition 1; 2) solving the subproblem (22) to obtain $\boldsymbol{a}$ using Algorithm 1; and 3) extending Algorithms 2 and 3 to the multiantenna cases. In the following, the convergence and complexity of our proposed four-step Algorithm 4 are analyzed.

At the zth iteration of Algorithm 4, the obtained solution is denoted by $(\boldsymbol{p}^{(z)}, a^{(z)}, \boldsymbol{v}^{(z)}, \boldsymbol{e}^{(z)})$. Then, the corresponding objective value can be given by $U^{(z)} = U(\boldsymbol{p}^{(z)}, a^{(z)}, \boldsymbol{v}^{(z)}, \boldsymbol{e}^{(z)})$. Owing to the continuous refinement of the solutions obtained by executing steps 1–4 in Algorithm 4, the objective value of the original problem (9) is nonincreasing. Meanwhile, considering the fact that the MSE value is lower bounded by zero and the number of devices is upper bounded by N, thus the sequence $\{U^{(z)}\}$ is lower bounded and is capable of at least converging to a locally optimal solution of the original MINLP problem (9), if not an optimal one.

When the reformulated subproblems are solved by CVX, the interior point method is considered, unless otherwise stated. For Algorithm 4, the main complexity of solving problem (9) lies in solving the phase-shifting design subproblem (36) with Algorithm 2 (i.e., step 3) as well as dealing with the device selection subproblem (44) with Algorithm 3 (i.e., step 4). More specifically, the dimension of variables to be solved in Algorithm 2 is $LM + 1$. Hence, the complexity is given by $\mathcal{O}(N_2(LM + 1)^3)$, where N_2 is the maximum iteration number to check feasibility. To solve the DC programming problem (41), the second-order interior point method [53] is adopted by Algorithm 3, and then the computational cost can be given as $\mathcal{O}(N_3(N + 1)^3)$, where N_3 is the maximum iteration number. As a result, the total complexity of solving the MINLP problem (10) with Algorithm 4 is $\mathcal{O}_1 = \mathcal{O}(N_2N_4(LM+1)^3+N_3N_4(N+1)^3)$, where N_4 is the maximum iteration number to obtain a converged solution. Regarding the complexity of solving problems in the multiantenna cases, it mainly depends on steps 2-3-4. In the second step, the complexity of Algorithm 1 consists of two parts: 1) the initial process and 2) the iterative process. Specifically, the complexity of solving problem (24) during the initialization is given by $\mathcal{O}((N_r^2+K)^{3.5})$ [51], and the complexity of solving the convex problem (27) at each iteration is given by $\mathcal{O}((N_r+2K)^3)$. Thus, the total complexity of solving problem (22) with Algorithm 1 is bounded by $\mathcal{O}((N_r^2 + K)^{3.5} + N_1(N_r + 2K)^3)$. Accordingly, the complexity of using an alternating optimization technique to solve problems in the multiantenna case can be given by $\mathcal{O}_2 = \mathcal{O}(N_4(N_r^2+K)^{3.5}+N_1N_4(N_r+2K)^3+N_2N_4(LM+1)^3+N_3N_4(N+1)^3)$.

VI. Experimental Settings and Results

A. Simulation Settings

As shown in Fig. 5, we consider that there are $N = 6$ IoT devices, $L = 3$ RISs, and one BS in the AirFL system,

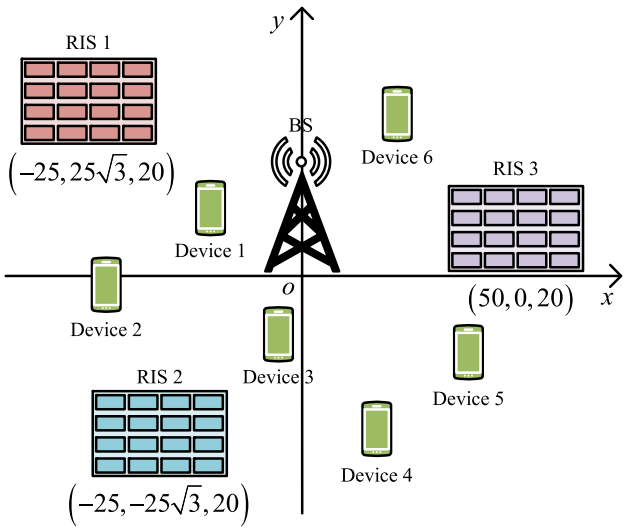

Fig. 5. Simulation setup of multi-RIS-aided AirFL systems (top view).

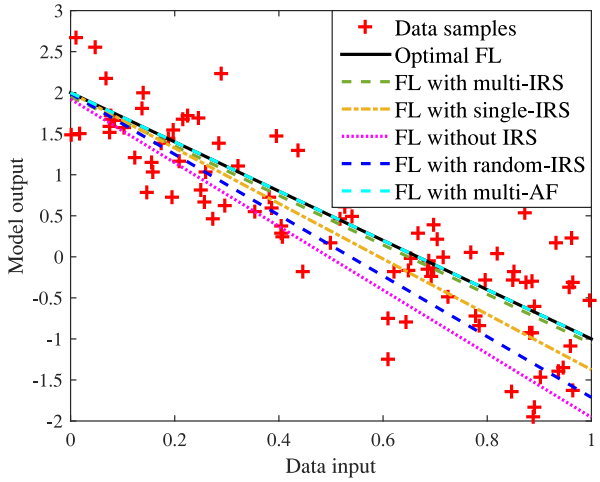

Fig. 6. Example of implementing FL for linear regression.

where all devices are uniformly distributed in a square area of size 100×100 (in meters) with the BS located at its center [20]. In the three-dimensional (3-D) Cartesian coordinates, the location of the ℓth RIS is given by $(x_\ell, y_\ell, z_\ell) = (50\cos(2\pi\ell/L), 50\sin(2\pi\ell/L), 20)$, and each RIS is equipped with $M = 60$ reflecting elements. It is assumed that all devices are on the horizontal plane, and the BS is located at $(0, 0, 25)$. Moreover, the maximum transmit power at each device is set as $P_0 = 23$ dBm, and the noise power is $\sigma^2 = -80$ dBm. Other parameters are set to $\gamma = 0.2$ and $\varepsilon_0 = 0.01$. The channel gain equals to the small-scale fading multiplied by the square root of the path loss, refer to [42] for specific settings of the channel model.

To verify the superiority of the designed algorithms for federated learning systems aided by multiple RISs (labeled "FL with multi-RIS"), we train a linear regression model in a federated manner to predict the relationship between the input x and the output y [26]. Note that x and y satisfy $y = -3x + 2 + 0.5 \times n_0$, where the input data x is randomly generated from $[0, 1]$, and the Gaussian noise n_0 follows $\mathcal{N}(0, 1)$. Specifically, the regress function in MATLAB is invoked to fit 30 on-device samples for linear regression at each iteration. Moreover, the proposed FL framework is also adopted to train a 6-layered convolutional neural network (CNN) for image classification on the MNIST data set, and a 50-layered residual network (ResNet) on the CIFAR-10 data set. For comparison purposes, the following four schemes are considered as benchmarks in our experiments.

1) *FL Without RIS:* Only one BS and N devices are considered in the federated learning system, where AirComp is adopted to compute specific functions via concurrent transmission over multiaccess channels.
2) *FL With Single-RIS:* Compared to the above scheme, one central RIS is deployed at $(50, 0, 20)$ to assist the model uploading from devices to the BS. For the fairness of comparison, the number of reflecting elements for the central RIS equals to $L \times M$.
3) *FL With Random-RIS:* The single RIS with random phase shifts is also considered as one benchmark. Note that the elements in $\boldsymbol{\theta}$ are randomly chosen from $[0, 2\pi]$, while other variables are solved by our proposed algorithms.
4) *FL With Multi-AF:* The deployment of multiple amplify-and-forward (AF) relays is the same as that of FL with multi-RIS scheme. Namely, there are three active AF relays that work in half-duplex mode, and each consists of M antennas.

B. Performance Evaluation

1) Implementing FL for Linear Regression: In Fig. 6, an ideal scheme called "optimal FL" is invoked to illustrate the performance upper bound, in which the communication conditions are perfect between the BS and devices, namely, the wireless noise is zero. Thus, the relationship between the input x and the output y can be modeled without error. One can notice that the proposed FL with multi-RIS scheme is capable of training a near-optimal model close to the ideal scheme. Compared with other benchmark schemes, such as "FL with single/random-RIS" and "FL without RIS," our scheme is able to fit data samples more accurately. This is largely due to the joint design of federated learning factors and wireless communication parameters. Besides, our scheme also carefully adjusts the reflection matrix of distributed RISs to suppress noise during the model aggregation process of federated learning. Then, Fig. 7 shows that the proposed scheme can converge faster to a smaller training loss, similar to the active scheme of "FL with multi-AF." This is mainly because the signal distortion caused by unfavorable wireless channels can be well mitigated by judiciously reconfiguring the propagation environment with the aid of multiple RISs. In Fig. 8, we can see that when the number of selected devices grows, the test error on the validation data set decreases to a low level. This comes from that the global model becomes more accurate if much more data samples are trained for aggregation. Thereby, the test error of all schemes is decreasing due to the improvement of prediction accuracy. One can observe from Fig. 9

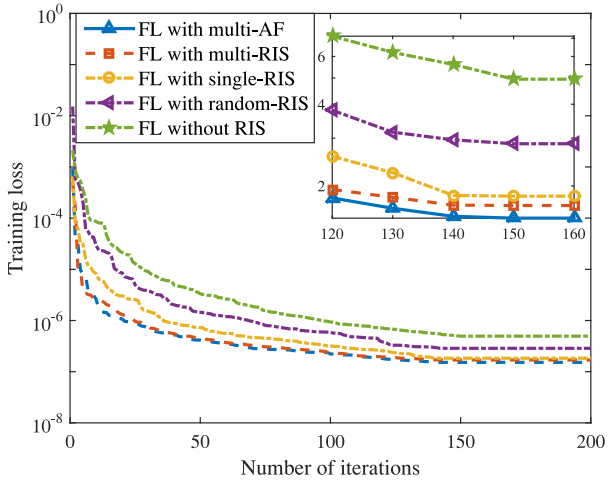

Fig. 7. Training loss versus the number of iterations.

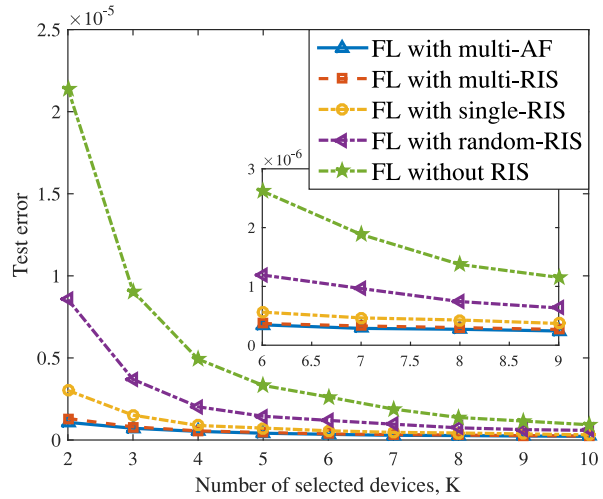

Fig. 8. Test error versus K.

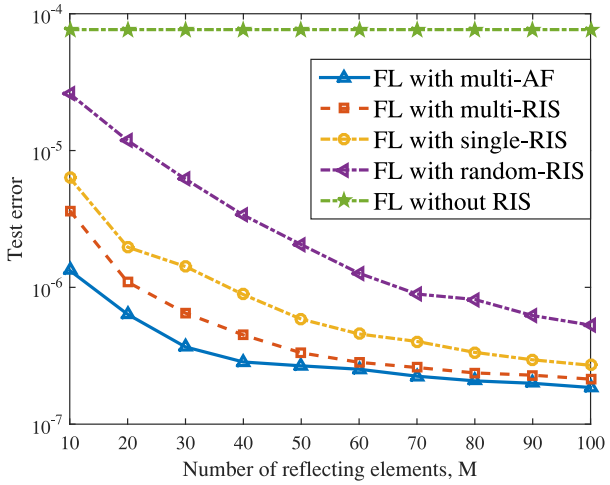

Fig. 9. Test error versus M.

that the test error decreases with the number of reflecting elements (or the number of antennas of each AF). This is due to the fact that a larger number of reflecting elements can lead to a smarter wireless environment and the propagation

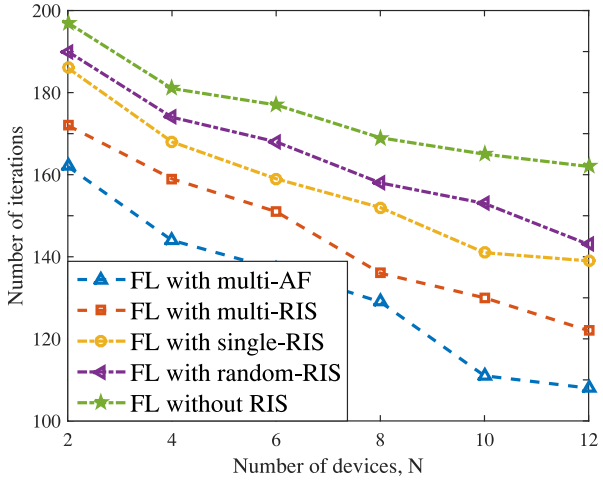

Fig. 10. Number of iterations versus N.

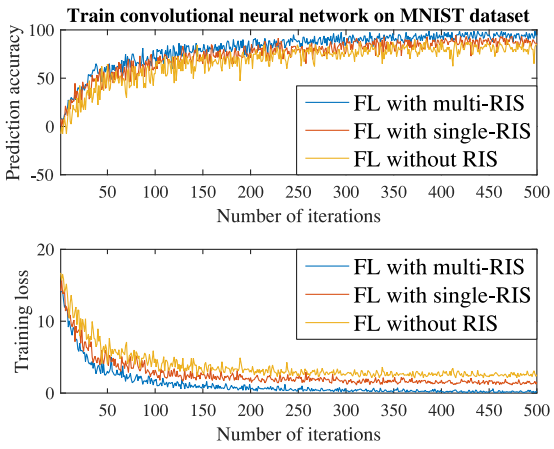

Fig. 11. Train CNN on the MNIST data set.

error induced from the channel noise can be suppressed more effectively. Finally, Fig. 10 illustrates that the number of iterations decreases as the number of devices increases. When the network size becomes larger, more devices can be selected to participate learning process, which accelerates the convergence of federated learning. Compared with other RIS-related benchmarks, the proposed scheme can work more efficiently and spend fewer communication rounds with the aided of multiple RISs.

2) Implementing FL for Image Classification: In Figs. 11 and 12, we evaluate the learning performance for image classification on real data in terms of training loss and prediction accuracy. Both the MNIST and CIFAR-10 data sets are divided into five training batches and one test batch, each with 10 000 images. The on-device CNN or ResNet is trained in parallel using randomly sampled images. To minimize loss, the SGD solver with an initial learning rate of 0.01 is adopted as an optimizer to update parameters at each iteration, where the size of each mini-batch is specified as 128. Compared to benchmarks, it is noted that the proposed scheme with multiple RISs can achieve lower training loss and higher prediction accuracy on both real data sets thanks to the reduced aggregation error.

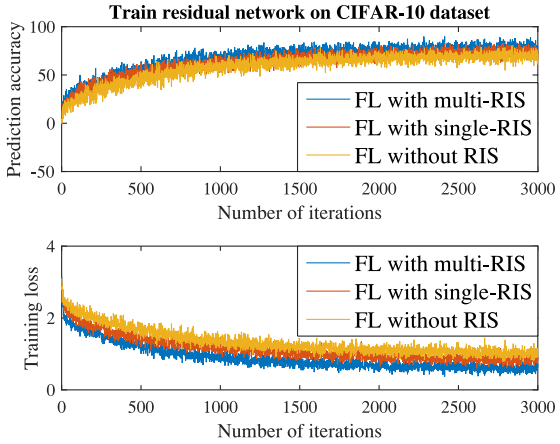

Fig. 12. Train ResNet on CIFAR-10 data.

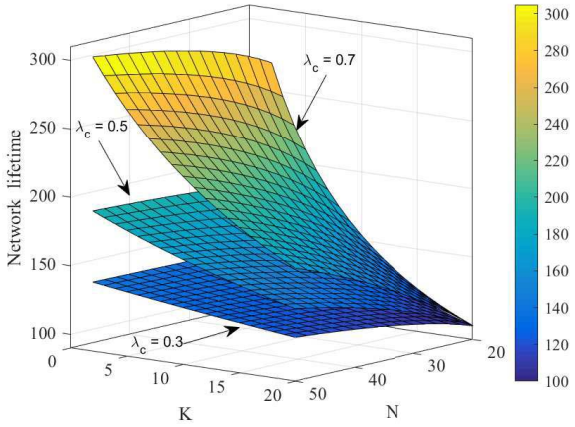

Fig. 13. Network lifetime versus K and N.

3) Network Lifetime of the Considered FL System: In Fig. 13, the impact of various K and N values on the network lifetime is demonstrated. In our simulation, if one device is selected to transmit its local parameters to the BS, it will spend 1 unit energy for data sensing, local computing, and communication processes, during which time the percentage of total energy consumption for communications is denoted by λ_c. Thus, the remaining processes require $1-\lambda_c$ unit energy regardless of whether the device communicates with the BS. Moreover, it is assumed that each device has $\delta = 100$ units energy, and the time until the first device dies is defined as the network lifetime, which can be given by $\lfloor N\delta/(N-\lambda_c N+\lambda_c K)\rfloor$, and $\lfloor\cdot\rfloor$ is the floor function. It can be seen from this figure that a higher λ_c leads to a longer network lifetime, i.e., more energy consumption for sensing and computing will shorten the network lifetime. Additionally, one can observe that the performance of network lifetime is positively proportional to N and is also inversely proportional to K. Namely, if more devices are deployed and less devices are selected, a longer network lifetime can be achieved. Therefore, the tradeoff between learning performance and network lifetime is an interesting research direction in future work.

VII. Conclusion

In this article, we investigated model aggregation and device selection problems of federated learning systems aided by distributed RISs. Considering the noisy fading channels, we jointly optimized the transmit power, receive scalar, phase shifts, and learning participants to minimize the aggregation error while accelerating the convergence rate of AirFL. To solve this challenging bicriterion problem, we derived closed-form solutions for the optimal transceiver design in the cases of a single antenna. Meanwhile, we provided iterative algorithms for the multiantenna cases by invoking relaxation methods, such as SDR, SCA, and DC programming. Accordingly, we proposed an alternating optimization algorithm to tackle the original MINLP problem for obtaining a suboptimal solution. Simulation results demonstrated that 1) the aggregation distortion can be effectively reduced by leveraging geodistributed intelligent surfaces to reconfigure the wireless channels; 2) the learning behavior of AirFL can be improved by the designed resource allocation and device selection algorithms; and 3) the designed alternating optimization algorithm is also capable of reducing energy consumption and prolonging the network lifetime of battery-constrained IoT networks.

Appendix A
Proof of Theorem 1

Due to the fact that $|a\bar{h}_k|^2 = |a|^2|\bar{h}_k|^2\ \forall k$, the constraints (18b) in problem (18) can be rewritten as $|a|^2 \geq |\bar{h}_k|^{-2}\ \forall k$. Thus, the problem (18) is reformulated as

$$\min_{a,\boldsymbol{\theta}}\ |a|^2 \tag{47a}$$

$$\text{s.t.}\ \ |a|^2 \geq \left|\bar{h}_k\right|^{-2} \quad \forall k \in \mathcal{K} \tag{47b}$$

$$(9c). \tag{47c}$$

It can be easily verified that at the optimal solution to problem (47), all the constraints in (47) should be met, i.e.,

$$\left|a^*\right| = \frac{1}{\min\limits_k \left|\bar{h}_k\right|} = \max_k \left|h_k + \sum_{\ell=1}^{L} \bar{\mathbf{g}}_\ell \boldsymbol{\Theta}_\ell \mathbf{g}_k^\ell\right|^{-1}. \tag{48}$$

Furthermore, it can be observed from (48) that the value of $|a^*|$ decreases as the value of $|\bar{h}_k|$ increases. As a result, the phase shifts of RISs should be finely tuned to render the phase shift of $\sum_{\ell=1}^{L} \bar{\mathbf{g}}_\ell \boldsymbol{\Theta}_\ell \mathbf{g}_k^\ell$ the same as that of h_k for all users, which can be expressed as $\arg(\sum_{\ell=1}^{L} \bar{\mathbf{g}}_\ell \boldsymbol{\Theta}_\ell^* \mathbf{g}_k^\ell) = \arg(h_k)\ \forall k \in \mathcal{K}$. This completes the proof of Theorem 1.

Appendix B
Proof of Lemma 1

According to the definitions of τ and $\bar{\rho}$ in Lemma 1, it holds that

$$\tau = \max_k \frac{\bar{\rho}}{\left|a\bar{h}_k\right|^2}. \tag{49}$$

Hence, it can be observed that the value of τ should be no less than $\bar{\rho}/|a\bar{h}_k|^2$ for all users, i.e., $\tau \geq \bar{\rho}/|a\bar{h}_k|^2\ \forall k \in \mathcal{K}$.

Then, problem (37) can be equivalently reformulated as

$$\min_{\mathcal{K},\tau} \quad \tau - |\mathcal{K}| \tag{50a}$$

$$\text{s.t.} \quad \tau \geq \frac{\bar{\rho}}{\left|a\bar{h}_k\right|^2} \quad \forall k \in \mathcal{K} \tag{50b}$$

$$|a|^2 - \rho\left|a\bar{h}_k\right|^2 \leq 0 \quad \forall k \in \mathcal{K} \tag{50c}$$

$$1 \leq |\mathcal{K}| \leq N \tag{50d}$$

where the objective and constraints in (50) are obviously equivalent to those in (38), and thus the proof of Lemma 1 is completed. Note that constraint (50b) holds with equality for at least one k of the optimal solution.

REFERENCES

[1] W. Ni, Y. Liu, and H. Tian, "Intelligent reflecting surfaces enhanced federated learning," in *Proc. IEEE GLOBECOM Workshops*, Taipei, Taiwan, Dec. 2020, pp. 1–6.

[2] M. Chen, U. Challita, W. Saad, C. Yin, and M. Debbah, "Artificial neural networks-based machine learning for wireless networks: A tutorial," *IEEE Commun. Surveys Tuts.*, vol. 21, no. 4, pp. 3039–3071, 4th Quart., 2019.

[3] J. Park, S. Samarakoon, M. Bennis, and M. Debbah, "Wireless network intelligence at the edge," *Proc. IEEE*, vol. 107, no. 11, pp. 2204–2239, Nov. 2019.

[4] K. Yang, Y. Shi, Y. Zhou, Z. Yang, L. Fu, and W. Chen, "Federated machine learning for intelligent IoT via reconfigurable intelligent surface," *IEEE Netw.*, vol. 34, no. 5, pp. 16–22, Sep./Oct. 2020.

[5] T. Li, A. K. Sahu, A. Talwalkar, and V. Smith, "Federated learning: Challenges, methods, and future directions," *IEEE Signal Process. Mag.*, vol. 37, no. 3, pp. 50–60, May 2020.

[6] Y. Shi, K. Yang, T. Jiang, J. Zhang, and K. B. Letaief, "Communication-efficient edge AI: Algorithms and systems," *IEEE Commun. Surveys Tuts.*, vol. 22, no. 4, pp. 2167–2191, 4th Quart., 2020.

[7] D. Gündüüz, D. B. Kurka, M. Jankowski, M. M. Amiri, E. Ozfatura, and S. Sreekumar, "Communicate to learn at the edge," *IEEE Commun. Mag.*, vol. 58, no. 12, pp. 14–19, Dec. 2020.

[8] X. Lyu, C. Ren, W. Ni, H. Tian, R. P. Liu, and E. Dutkiewicz, "Optimal online data partitioning for geo-distributed machine learning in edge of wireless networks," *IEEE J. Sel. Areas Commun.*, vol. 37, no. 10, pp. 2393–2406, Oct. 2019.

[9] Y. Liu, S. Bi, Z. Shi, and L. Hanzo, "When machine learning meets big data: A wireless communication perspective," *IEEE Veh. Technol. Mag.*, vol. 15, no. 1, pp. 63–72, Mar. 2020.

[10] M. Chen, N. Shlezinger, H. V. Poor, Y. C. Eldar, and S. Cui, "Communication-efficient federated learning," *Proc. Nat. Acad. Sci.*, vol. 118, no. 17, pp. 1–8, Apr. 2021.

[11] M. Chen, H. V. Poor, W. Saad, and S. Cui, "Wireless communications for collaborative federated learning," *IEEE Commun. Mag.*, vol. 58, no. 12, pp. 48–54, Dec. 2020.

[12] D. Liu and O. Simeone, "Privacy for free: Wireless federated learning via uncoded transmission with adaptive power control," *IEEE J. Sel. Areas Commun.*, vol. 39, no. 1, pp. 170–185, Jan. 2021.

[13] B. Nazer and M. Gastpar, "Computation over multiple-access channels," *IEEE Trans. Inf. Theory*, vol. 53, no. 10, pp. 3498–3516, Oct. 2007.

[14] H. Guo, A. Liu, and V. K. N. Lau, "Analog gradient aggregation for federated learning over wireless networks: Customized design and convergence analysis," *IEEE Internet Things J.*, vol. 8, no. 1, pp. 197–210, Jan. 2021.

[15] G. Zhu, J. Xu, K. Huang, and S. Cui, "Over-the-air computing for wireless data aggregation in massive IoT," *IEEE Wireless Commun.*, vol. 28, no. 4, pp. 57–65, Aug. 2021.

[16] G. Zhu, Y. Wang, and K. Huang, "Broadband analog aggregation for low-latency federated edge learning," *IEEE Trans. Wireless Commun.*, vol. 19, no. 1, pp. 491–506, Jan. 2020.

[17] M. Chen, H. V. Poor, W. Saad, and S. Cui, "Convergence time optimization for federated learning over wireless networks," *IEEE Trans. Wireless Commun.*, vol. 20, no. 4, pp. 2457–2471, Apr. 2021.

[18] G. Zhu, D. Liu, Y. Du, C. You, J. Zhang, and K. Huang, "Toward an intelligent edge: Wireless communication meets machine learning," *IEEE Commun. Mag.*, vol. 58, no. 1, pp. 19–25, Jan. 2020.

[19] Y. Liu *et al.*, "Reconfigurable intelligent surfaces: Principles and opportunities," *IEEE Commun. Surveys Tuts.*, vol. 23, no. 3, pp. 1546–1577, 3rd Quart., 2021, doi: 10.1109/COMST.2021.3077737.

[20] Z. Yang, M. Chen, W. Saad, C. S. Hong, and M. Shikh-Bahaei, "Energy efficient federated learning over wireless communication networks," *IEEE Trans. Wireless Commun.*, vol. 20, no. 3, pp. 1935–1949, Mar. 2021.

[21] Q. Wu and R. Zhang, "Intelligent reflecting surface enhanced wireless network via joint active and passive beamforming," *IEEE Trans. Wireless Commun.*, vol. 18, no. 11, pp. 5394–5409, Nov. 2019.

[22] W. Ni, Y. Liu, Z. Yang, H. Tian, and X. Shen, "Integrating over-the-air federated learning and non-orthogonal multiple access: What role can RIS play?" Mar. 2021. *arxiv:2103.00435*.

[23] C. Xu, S. Liu, Z. Yang, Y. Huang, and K.-K. Wong, "Learning rate optimization for federated learning exploiting over-the-air computation," *IEEE J. Sel. Areas Commun.*, vol. 39, no. 12, pp. 3742–3756, Dec. 2021.

[24] W. Ni, Y. Liu, Y. C. Eldar, Z. Yang, and H. Tian, "STAR-RIS enabled heterogeneous networks: Ubiquitous NOMA communication and pervasive federated learning," Jun. 2021, *arxiv:2106.08592*.

[25] M. M. Amiri and D. Gündüz, "Federated learning over wireless fading channels," *IEEE Trans. Wireless Commun.*, vol. 19, no. 5, pp. 3546–3557, May 2020.

[26] M. Chen, Z. Yang, W. Saad, C. Yin, H. V. Poor, and S. Cui, "A joint learning and communications framework for federated learning over wireless networks," *IEEE Trans. Wireless Commun.*, vol. 20, no. 1, pp. 269–283, Jan. 2021.

[27] L. Chen, N. Zhao, Y. Chen, F. R. Yu, and G. Wei, "Over-the-air computation for IoT networks: Computing multiple functions with antenna arrays," *IEEE Internet Things J.*, vol. 5, no. 6, pp. 5296–5306, Dec. 2018.

[28] W. Liu, X. Zang, Y. Li, and B. Vucetic, "Over-the-air computation systems: Optimization, analysis and scaling laws," *IEEE Trans. Wireless Commun.*, vol. 19, no. 8, pp. 5488–5502, Aug. 2020.

[29] K. Yang, T. Jiang, Y. Shi, and Z. Ding, "Federated learning via over-the-air computation," *IEEE Trans. Wireless Commun.*, vol. 19, no. 3, pp. 2022–2035, Mar. 2020.

[30] J. Ren, Y. He, D. Wen, G. Yu, K. Huang, and D. Guo, "Scheduling for cellular federated edge learning with importance and channel awareness," *IEEE Trans. Wireless Commun.*, vol. 19, no. 11, pp. 7690–7703, Nov. 2020.

[31] X. Li, G. Zhu, Y. Gong, and K. Huang, "Wirelessly powered data aggregation for IoT via over-the-air function computation: Beamforming and power control," *IEEE Trans. Wireless Commun.*, vol. 18, no. 7, pp. 3437–3452, Jul. 2019.

[32] C. Huang, A. Zappone, G. C. Alexandropoulos, M. Debbah, and C. Yuen, "Reconfigurable intelligent surfaces for energy efficiency in wireless communication," *IEEE Trans. Wireless Commun.*, vol. 18, no. 8, pp. 4157–4170, Aug. 2019.

[33] H. Xie, J. Xu, and Y.-F. Liu, "Max-min fairness in IRS-aided multi-cell MISO systems with joint transmit and reflective beamforming," *IEEE Trans. Wireless Commun.*, vol. 20, no. 2, pp. 1379–1393, Feb. 2021.

[34] C. Huang, R. Mo, and C. Yuen, "Reconfigurable intelligent surface assisted multiuser MISO systems exploiting deep reinforcement learning," *IEEE J. Sel. Areas Commun.*, vol. 38, no. 8, pp. 1839–1850, Aug. 2020.

[35] H. Zhang, B. Di, L. Song, and Z. Han, "Reconfigurable intelligent surfaces assisted communications with limited phase shifts: How many phase shifts are enough?" *IEEE Trans. Veh. Technol.*, vol. 69, no. 4, pp. 4498–4502, Apr. 2020.

[36] T. Hou, Y. Liu, Z. Song, X. Sun, and Y. Chen, "MIMO-NOMA networks relying on reconfigurable intelligent surface: A signal cancellation based design," *IEEE Trans. Commun.*, vol. 68, no. 11, pp. 6932–6944, Nov. 2020.

[37] Y. Cheng, K. H. Li, Y. Liu, K. C. Teh, and H. V. Poor, "Downlink and uplink intelligent reflecting surface aided networks: NOMA and OMA," *IEEE Trans. Wireless Commun.*, vol. 20, no. 6, pp. 3988–4000, Jun. 2021.

[38] Z. Li *et al.*, "Energy efficient reconfigurable intelligent surface enabled mobile edge computing networks with NOMA," *IEEE Trans. Cogn. Commun. Netw.*, vol. 7, no. 2, pp. 427–440, Jun. 2021.

[39] Z. Tang, T. Hou, Y. Liu, J. Zhang, and C. Zhong, "A novel design of RIS for enhancing the physical layer security for RIS-aided NOMA networks," *IEEE Wireless Commun. Lett.*, vol. 10, no. 11, pp. 2398–2401, Nov. 2021.

[40] J. Zuo, Y. Liu, Z. Qin, and N. Al-Dhahir, "Resource allocation in intelligent reflecting surface assisted NOMA systems," *IEEE Trans. Commun.*, vol. 68, no. 11, pp. 7170–7183, Nov. 2020.

[41] X. Liu, Y. Liu, Y. Chen, and H. V. Poor, "RIS enhanced massive non-orthogonal multiple access networks: Deployment and passive beamforming design," *IEEE J. Sel. Areas Commun.*, vol. 39, no. 4, pp. 1057–1071, Apr. 2021.
[42] W. Ni, X. Liu, Y. Liu, H. Tian, and Y. Chen, "Resource allocation for multi-cell IRS-aided NOMA networks," *IEEE Trans. Wireless Commun.*, vol. 20, no. 7, pp. 4253–4268, Jul. 2021.
[43] T. Jiang and Y. Shi, "Over-the-air computation via intelligent reflecting surfaces," in *Proc. IEEE GLOBECOM*, Waikoloa, HI, USA, Dec. 2019, pp. 1–6.
[44] S. Wang *et al.*, "Adaptive federated learning in resource constrained edge computing systems," *IEEE J. Sel. Areas Commun.*, vol. 37, no. 6, pp. 1205–1221, Jun. 2019.
[45] G. Zhu and K. Huang, "MIMO over-the-air computation for high-mobility multimodal sensing," *IEEE Internet Things J.*, vol. 6, no. 4, pp. 6089–6103, Aug. 2019.
[46] L. Chen, X. Qin, and G. Wei, "A uniform-forcing transceiver design for over-the-air function computation," *IEEE Wireless Commun. Lett.*, vol. 7, no. 6, pp. 942–945, Dec. 2018.
[47] J.-Y. Gotoh, A. Takeda, and K. Tono, "DC formulations and algorithms for sparse optimization problems," *Math. Program.*, vol. 169, no. 1, pp. 141–176, May 2018.
[48] L. Wei, C. Huang, G. C. Alexandropoulos, C. Yuen, Z. Zhang, and M. Debbah, "Channel estimation for ris-empowered multi-user MISO wireless communications," *IEEE Trans. Commun.*, vol. 69, no. 6, pp. 4144–4157, Jun. 2021.
[49] H. Liu, X. Yuan, and Y.-J. A. Zhang, "Matrix-calibration-based cascaded channel estimation for reconfigurable intelligent surface assisted multiuser MIMO," *IEEE J. Sel. Areas Commun.*, vol. 38, no. 11, pp. 2621–2636, Nov. 2020.
[50] M. Grant and S. Boyd. "CVX: MATLAB Software for Disciplined Convex Programming, Version 2.1." Mar. 2014. [Online]. Available: http://cvxr.com/cvx
[51] Z.-Q. Luo, W.-K. Ma, A. Man-Cho So, Y. Ye, and S. Zhang, "Semidefinite relaxation of quadratic optimization problems," *IEEE Signal Process. Mag.*, vol. 27, no. 3, pp. 20–34, May 2010.
[52] Y. Sun, P. Babu, and D. P. Palomar, "Majorization–minimization algorithms in signal processing, communications, and machine learning," *IEEE Trans. Signal Process.*, vol. 65, no. 3, pp. 794–816, Feb. 2017.
[53] S. Boyd and L. Vandenberghe, *Convex Optimization*. Cambridge, U.K.: Cambridge Univ. Press, 2004.

Wanli Ni (Graduate Student Member, IEEE) received the B.E. degree in communication engineering from Beijing University of Posts and Telecommunications (BUPT), Beijing, China, in 2018, where he is currently pursuing the Ph.D. degree with the State Key Laboratory of Networking and Switching Technology.

Since 2020, he has been a visiting student (online) with the School of Electronic Engineering and Computer Science, Queen Mary University of London, London, U.K., under the supervision of Dr. Y. Liu. His current research interests include over-the-air federated learning, reconfigurable intelligent surface, and nonorthogonal multiple access.

Mr. Ni was a recipient of the Samsung Scholarship in 2019, the Best Paper Award from IEEE SAGC in 2020, the National Scholarship in 2021, and the Student Travel Grant from IEEE GLOBECOM in 2021.

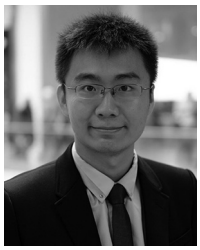

Yuanwei Liu (Senior Member, IEEE) received the B.S. and M.S. degrees from Beijing University of Posts and Telecommunications, Beijing, China, in 2011 and 2014, respectively, and the Ph.D. degree in electrical engineering from the Queen Mary University of London, London, U.K., in 2016.

He was with the Department of Informatics, King's College London, London, from 2016 to 2017, where he was a Postdoctoral Research Fellow. He has been a Senior Lecturer (Associate Professor) with the School of Electronic Engineering and Computer Science, Queen Mary University of London since August 2021, where he was a Lecturer (Assistant Professor) from 2017 to 2021. His research interests include nonorthogonal multiple access, 5G/6G networks, machine learning, and stochastic geometry.

Dr. Liu received the IEEE ComSoc Outstanding Young Researcher Award for EMEA in 2020, the 2020 Early Achievement Award of the IEEE ComSoc Signal Processing and Computing for Communications (SPCC) Technical Committee, the 2021 Early Achievement Award of IEEE Communication Theory Technical Committee, and the Exemplary Reviewer Certificate of IEEE WIRELESS COMMUNICATIONS LETTERS in 2015, IEEE TRANSACTIONS ON COMMUNICATIONS in 2016 and 2017, and IEEE TRANSACTIONS ON WIRELESS COMMUNICATIONS in 2017 and 2018. He is a Web of Science Highly Cited Researcher in 2021. He is currently a Senior Editor of IEEE COMMUNICATIONS LETTERS, and an Editor of the IEEE TRANSACTIONS ON WIRELESS COMMUNICATIONS and the IEEE TRANSACTIONS ON COMMUNICATIONS. He serves as the leading Guest Editor for IEEE JSAC special issue on Next Generation Multiple Access, and a Guest Editor for IEEE JSTSP special issue on Signal Processing Advances for Nonorthogonal Multiple Access in Next Generation Wireless Networks. He has served as a TPC Member for many IEEE conferences, such as GLOBECOM and ICC. He has served as the Publicity Co-Chair for VTC 2019-Fall. He serves as the Chair for Special Interest Group in SPCC Technical Committee on the topic of Signal Processing Techniques for Next-Generation Multiple Access, the Vice-Chair for SIG Wireless Communications Technical Committee on the topic of Reconfigurable Intelligent Surfaces for Smart Radio Environments, and the Tutorials and the Invited Presentations Officer for Reconfigurable Intelligent Surfaces Emerging Technology Initiative.

Zhaohui Yang (Member, IEEE) received the B.S. degree in information science and engineering from Chien-Shiung Wu Honors College, Southeast University, Nanjing, China, in June 2014, and the Ph.D. degree in communication and information system from the National Mobile Communications Research Laboratory, Southeast University in May 2018.

From May 2018 to October 2020, he was a Postdoctoral Research Associate with the Center for Telecommunications Research, Department of Informatics, King's College London, London, U.K. He is currently a Visiting Associate Professor with the College of Information Science and Electronic Engineering, Zhejiang Key Laboratory of Information Processing Communication and Networking, Zhejiang University, Hangzhou, China, and also a Research Fellow with the Department of Electronic and Electrical Engineering, University College London, London. His research interests include federated learning, reconfigurable intelligent surface, UAV, and NOMA.

Dr. Yang is an Associate Editor of the IEEE COMMUNICATIONS LETTERS, *IET Communications*, and *EURASIP Journal on Wireless Communications and Networking*. He has guest edited a feature topic of *IEEE Communications Magazine* on Communication Technologies for Efficient Edge Learning. He was a TPC Member of IEEE ICC from 2015 to 2021 and GLOBECOM from 2017 to 2021. He was an Exemplary Reviewer of IEEE TRANSACTIONS ON COMMUNICATIONS in 2019 and 2020.

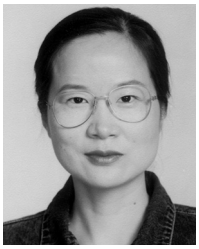

Hui Tian (Senior Member, IEEE) received the M.S. and Ph.D. degrees from Beijing University of Posts and Telecommunications (BUPT), Beijing, China, in 1992 and 2003, respectively.

She is currently a Professor with BUPT. Her current research interests mainly include radio resource management in 5G/6G networks, mobile-edge computing, cooperative communication, mobile social network, and Internet of Things.

Xuemin (Sherman) Shen (Fellow, IEEE) received the Ph.D. degree in electrical engineering from Rutgers University, New Brunswick, NJ, USA, in 1990.

He is a University Professor with the Department of Electrical and Computer Engineering, University of Waterloo, Waterloo, ON, Canada. His research focuses on network resource management, wireless network security, Internet of Things, 5G and beyond, and vehicular networks.

Dr. Shen received the Canadian Award for Telecommunications Research from the Canadian Society of Information Theory in 2021, the R.A. Fessenden Award in 2019 from IEEE, Canada, the Award of Merit from the Federation of Chinese Canadian Professionals (Ontario) in 2019, the James Evans Avant Garde Award in 2018 from the IEEE Vehicular Technology Society, the Joseph LoCicero Award in 2015 and Education Award in 2017 from the IEEE Communications Society (ComSoc), and the Technical Recognition Award from Wireless Communications Technical Committee in 2019 and AHSN Technical Committee in 2013. He has also received the Excellent Graduate Supervision Award in 2006 from the University of Waterloo and the Premier's Research Excellence Award in 2003 from the Province of Ontario, Canada. He served as the Technical Program Committee Chair/Co-Chair for IEEE GLOBECOM'16, IEEE INFOCOM'14, IEEE VTC'10 Fall, and IEEE GLOBECOM'07, and the Chair for the IEEE ComSoc Technical Committee on Wireless Communications. He is the President Elect of the IEEE ComSoc. He was the Vice President for Technical & Educational Activities and Publications, a Member-at-Large on the Board of Governors, the Chair of the Distinguished Lecturer Selection Committee, and a member of IEEE Fellow Selection Committee of the ComSoc. He served as the Editor-in-Chief for the IEEE INTERNET OF THINGS JOURNAL, IEEE NETWORK, and *IET Communications*. He is a registered Professional Engineer of Ontario, Canada, an Engineering Institute of Canada Fellow, a Canadian Academy of Engineering Fellow, a Royal Society of Canada Fellow, a Chinese Academy of Engineering Foreign Member, and a Distinguished Lecturer of the IEEE Vehicular Technology Society and Communications Society.